TE SCATTERING FROM A DIELECTRIC COATED CONDUCTING STRIP

THESIS

William D. Wood, Jr.
Captain, USAF

AFIT/GE/ENG/90D-67

DEPARTMENT OF THE AIR FORCE
AIR UNIVERSITY
AIR FORCE INSTITUTE OF TECHNOLOGY
Wright-Patterson Air Force Base, Ohio

AFIT/GE/ENG/90D-67

TE SCATTERING FROM A DIELECTRIC COATED CONDUCTING STRIP

THESIS

William D. Wood, Jr.
Captain, USAF

AFIT/GE/ENG/90D-67

AFIT/GE/ENG/90D-67

TE SCATTERING FROM A DIELECTRIC COATED CONDUCTING STRIP

THESIS

Presented to the Faculty of the School of Engineering

of the Air Force Institute of Technology

Air University

In Partial Fulfillment of the

Requirements for the Degree of

Master of Science in Electrical Engineering

William D. Wood, Jr., B.S E.E.

Captain, USAF

December, 1990

Approved for public release; distribution unlimited

Preface

When I began this research effort 12 months ago, I saw it as merely an obstacle between myself and graduation; somewhere along the way it became much more than that Would I have believed four quarters ago that I would be sorry when it ended?

Far from being an individual effort, many people provided invaluable assistance and their names deserve to appear on this document as much as mine First and foremost, I would like to thank Maj Harry Barksdale, my advisor, for his expert technical help and, more importantly, always taking the time to listen to even my most foolish ideas. He also originated the change of variables upon which this thesis centrally relies The members of my thesis committee, Capts Philip Joseph and Byron Welsh, deserve thanks for providing much-needed feedback and technical advice I would also like to thank Dr Fred Tokarz, ASD/ENAMA, for sponsoring this thesis, I only hope that some of his questions have been answered.

I owe a special debt of gratitude to Dr Bill Kent of Mission Research Corporation (MRC) His enthusiasm and technical insights into the nature of physical basis functions were of inestimable help. I am also indebted to Dr Ron Riechers and Mr Adam Berning of MRC for their mathematical insights and computer expertise.

William D. Wood, Jr.

Table of Contents

List of Figures

List of Tables

Abstract

Consider a plane wave incident on a conducting strip of infinite length coated on one side with a thin, uniform coating of lossless dielectric, and let the incident magnetic field vector be parallel to the edges of the strip. From first principles we develop the integral equations relating the total, incident, and scattered fields in the dielectric We expand the fields in the dielectric slab as the sum of three plane waves (the "forced" wave and two oppositely-directed surface waves) The phase constants in the $\hat{x}$ and $\hat{y}$ directions are known and the wave amplitudes are found using least-squared-error point-matching.

The far-zone scattered field is found by letting the polarization and conduction currents radiate in free space.

Data are presented showing the bistatic scattering characteristics of the dielectric-coated conducting strip as a function of dielectric permittivity, slab width and thickness, and angle of incidence Results show reasonable agreement with conventional moment method solution using pulse bases and Galerkin testing functions.

TE SCATTERING FROM A DIELECTRIC COATED CONDUCTING STRIP

I. Introduction

1.1 Background

Today's military environment increasingly requires tactical and strategic aircraft to possess some measure of "stealth," or low-observable, capability The logic is intuitive if an aircraft cannot be detected, then it cannot be shot down, and hence is more effective than a conventional aircraft

The most potent threat an aircraft faces is acquisition/tracking radar in concert with either an infrared- or radar-guided missile Accordingly, most of the emphasis in the low-observables community has been aimed at reducing the radar cross section (RCS) of aircraft. The RCS of an aircraft is a measure of how much electromagnetic (EM) energy is reflected (scattered) back at an illuminating radar. Reducing an aircraft's RCS reduces the range at which a radar can detect it. Although actual RCS measurements for current military aircraft are classified, a reasonable estimate is that the RCS of newly-developed low-observable aircraft is comparable to that of a metal sphere that is 10 centimeters in diameter (very small indeed!) (13:22-23).

Reducing an aircraft's RCS is best approached using a "divide and conquer" approach An aircraft may be thought of as a collection of sections, each of which has an RCS associated with it The RCS of the total aircraft is then the coherent combination of the individual RCS's This partitioning has two advantages.

First, if one section of an aircraft has an RCS that dominates the RCS of all other sections, then the most benefit can be attained by concentrating efforts to reducing the RCS of that one dominant section.

Second, transforming the problem from the analysis of an extremely complex structure such as an aircraft to that of a relatively simple shape greatly reduces the difficulty of the problem In most cases, only a few canonical shapes (e.g , cylinders, plates, and spheroids) are necessary to adequately model an aircraft of arbitrary configuration

In the same manner that an aircraft is decomposed into canonical shapes, the RCS of the canonical shapes may be decomposed into various physical phenomena, called scattering mechanisms. In general, the scattering mechanisms of any object are dependent on the size, shape, and material properties of the object.

1.2 Statement of the Problem

One canonical shape of considerable interest is a conducting strip covered on one side with a thin material coating of known electrical properties For example, such a geometry can be used to model an aircraft section covered by radar-absorbing material (RAM), or even an airfoil covered with ice (6:3-4)

The specific problem (14 194-202) to be analyzed in this thesis is the electromagnetic scattering from a dielectric-coated conducting strip of infinite length, as shown in Figure 1 The strip

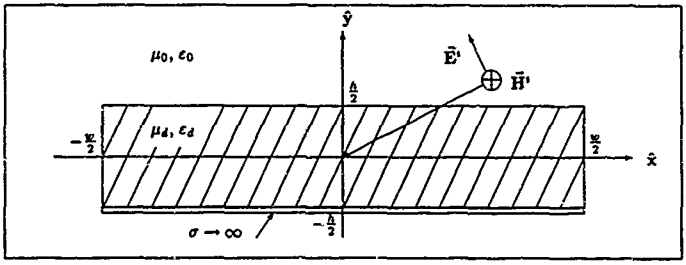

Figure 1. Two-Dimensional Scattering Geometry

is arbitrarily thin, has infinite conductivity σ, and finite width w. The dielectric coating has width w, thickness h, permittivity $\epsilon_d = \epsilon_r \epsilon_0$ and permeability $\mu_d = \mu_r \mu_0$ The incident field is a linearly

polarized, uniform plane wave of unit amplitude having the electric field vector transverse to the z-axis, i.e., in the transverse electric (TE) sense ($\vec{E}$ in the xy-plane, $\vec{H}$ aligned with the z-axis)

1.3 Approach

The first task consists of reviewing the available literature concerning electromagnetic scattering from coated objects The results are compiled in Chapter II.

The second task consists of developing the integral equations relating the scattered field to the incident field The total field quantities must satisfy the Helmholtz equation as well as the classical boundary conditions of $\vec{E}_z^T = 0$ at $y = -\frac{b}{2}$ and $\vec{E}_z^T$ and $\vec{H}_z^T$ continuous across $y = \frac{b}{2}$ (Fig 1) The results comprise Chapter III.

The third task is to develop a moment method solution to the integral equations using physical basis functions. The physical basis functions will consist of a forced wave and forward and reverse x-directed surface wave components (19). Testing functions will be oversampled point-matching Dirac delta functions, creating an over-determined linear system of equations and a non-square impedance matrix. Computer algorithms will be developed to generate the impedance matrix elements, which will be line and surface dimensional integrals involving Hankel functions of the second kind of order 0 The integrals will contain singularities which must be evaluated in the principal-value sense The over-determined system will be solved in the least-square-error sense using matrix pseudo-inversion techniques. The results may be found in Chapter IV.

The fourth task is to compare the output of the moment method algorithms developed in the second task to the output from a standard moment method program using pulse basis/point-matching. The criteria for comparison will be absolute accuracy of the solution, computer run time, and computer storage requirements If physical basis functions work as anticipated, the accuracies will be nearly identical, but the physical basis function solution will require much less computer time and storage than the standard moment method solution.

II. Literature Review

Much work has been done in the areas of "high-frequency" scattering theory – Geometrical Optics (GO), the Geometrical and Uniform Theories of Diffraction (GTD & UTD), Physical Optics (PO), and the Physical Theory of Diffraction (PTD) are the most prevalent. These methods are called "high-frequency" because they are derived from asymptotic solutions to the scattering equations in the limit as the wavelength of incident radiation becomes small compared to the dimensions of scatterer. In this thesis, however, the scatter is on the order of a wavelength (a few to tens of wavelengths in width) so the "high-frequency" methods are not strictly applicable. Therefore, only material dealing with the method of moments implementation will be reviewed. The review divides into two distinct portions: material dealing with developing the exact scattering integral equations, and that dealing with approximating the solution to the integral equation.

2.1 Integral Equations

The integral equations relating the scattered electric field $\vec{E}^s$ to the incident electric field $\vec{E}^i$ may be derived using several techniques; all are based on fundamental EM theory and are exact. In general, developing the integral equation is a two-step process.

2.1.1 Equivalent Currents. As a first step, we may remove the conducting portion of the scattering body and replace it with free space and equivalent electric and magnetic surface currents, J and M, on the external boundaries of the body (2, 10, 14, 21). This is a direct application of the surface equivalence theorem (3:329-333).

The surface currents are such that they radiate $\vec{E}^s$ outside the conducting scattering body and $-\vec{E}^i$ within it. This creates (necessarily) a vanishing field inside the conducting body, the technique is sometimes referred to as the "null field" approach (28). In addition, the fields radiated by the surface currents must satisfy the appropriate boundary conditions:

1. Continuity of the tangential electric and magnetic fields at a dielectric interface.

2. Vanishing tangential electric field at the surface of a perfect conductor.

In a similar manner, we may replace the dielectric portion of the scatterer by free space and equivalent volumetric current densities. These volumetric currents must satisfy the same boundary conditions as the surface currents. Once the surface and volume currents are specified, the scattered fields $\vec{E}^s$ may be easily found (21, 22). The problem is thus converted into finding the equivalent surface currents J and M in terms of the incident field $\vec{E}^i$

2.1.2 Integral Equation Formulation The second step is to formulate the integral equations for equivalent currents J and M. There are many ways to write the integral equations; the method used is influenced by the nature of the scattering body, the polarization of the incident field $\vec{E}^i$, or even the personal whims of the author.

Kent (14) uses Rumsey's Reaction Integral Equation for the specific cases of a finite-length dielectric-coated wire, an infinite dielectric slab, and a dielectric-coated conducting strip. Rogers (21) uses the dyadic free-space Green's function to write an integral equation defining the surface currents J and M. Use of dyadics is dictated by the arbitrary polarization of the incident field $\vec{E}^i$. Rogers asserts that the resulting equation is general and can be manipulated into Mitschang's vector and scalar potential function, the electric field integral equation (EFIE), the magnetic field integral equation (MFIE), and the combined field integral equation (CFIE). Huddleston (10) uses a CFIE formulation in which the scattered field $\vec{E}^s$ is expressed in terms of integrodifferential operators involving dyadic free-space Green's functions. Rojas (22) examines the inhomogeneous dielectric cylindrical scatterer; he uses the volume equivalence theorem (3:327-329) to define volumetric current densities within the cylinder in a manner analogous to that involving surface current densities. Again, Rojas' solution uses the dyadic free-space Green's function in the final integral equation. Arvas (2) uses the standard EFIE solution for the scattering from multiple perfectly conducting and lossy dielectric cylinders of arbitrary cross-section, including dielectric-coated conducting cylinders

2.2 *Method of Moments*

Once the integral equation is written, we must solve it to find the scattered field $\vec{E}^s$ in terms of the incident field $\vec{E}^i$. As stated earlier, no analytic, closed-form solution exists in general, and we must employ numerical techniques to approximate a solution. The preferred technique, called the Method of Moments (9), is to transform the integral equation into a system of linear algebraic equations This is done by expanding the unknown currents in basis functions and then introducing testing functions. Commonly, the same expansion functions are used as both basis and testing functions; this is known as Galerkin's method.

2.2.1 Subsectional Basis Functions Basis functions which exist only on discrete positional subsections are known as subsectional basis functions (3:683) Examples include pulses and piecewise sinusoids for two-dimensional geometries, and square and triangular patches for three-dimensional geometries. Subsectional basis functions provide the flexibility necessary to analyze arbitrary geometries where the nature of J and M is not known. However, solutions using subsectional basis functions typically require a large number of them to achieve a given level of accuracy in the solution.

Huddleston (10) uses two-dimensional triangular basis functions and Galerkin testing functions to expand the surface currents for coated and uncoated spheres, closed circular cylinders, and flat-back circular cones. Rogers (21) uses bi-triangular basis functions for the case of coated and uncoated flat square plates Arvas (2) and Rojas (22) use pulse basis/point matching to analyze several varied two-dimensional geometries involving dielectric and/or conducting cylinders

Most authors are eager to report agreement with measured and/or other published data but seem less enthusiastic to discuss the number of sub-domain basis functions N or the computer time and storage requirements necessary to achieve their results. Only Rojas (22) states the number of expansion functions N and the computer run-time needed to run his code. For example, he relates that for a circular-shell dielectric cylinder, the system of linear equations to be solved is of order

$N = 246$ and the computer code requires 3 minutes to run on a VAX 11/780.

2.2.2 Entire-Domain Basis Functions Basis functions which expand the unknown surface currents J and M into "modes" which exist over the entire scattering body are known as entire-domain basis functions Examples include Fourier series and Chebyshev polynomials Entire-domain basis functions require knowledge of the nature of unknown J and M, but can greatly reduce the order N of the system to be solved (3.685).

Kent (14) uses a special form of the entire-domain basis function called the physical basis function (PBF), introduced by Richmond in 1983 (19). PBFs can be used to

> analyze particular structures which may be large in one dimension but which will require only a small number of expansion functions for the unknown currents. The method will have the additional property that most or all of the current components have specific physical interpretations...

Specifically, Kent models the equivalent polarization and conduction currents

> as being composed of a 'forced' wave (which is similar to the classical physical optics (PO) current) and two oppositely directed surface waves.

Using PBFs and Galerkin testing functions, the order of the system of equations is N=3, a very small number indeed compared to subsectional basis functions. The price paid is the increased complexity of the numerical integrations which must be performed to fill the 3×3 impedance matrix.

For the dielectric-coated wire, Kent states that the PBF solution agrees well with the standard moment method solution using subsectional piecewise-sinusoidal (PWS) expansion functions for scatterer length greater than two wavelengths Some disagreement exists for shorter lengths; Kent suggests that a traveling wave current exists on the structure which is not accounted for in the PBF solution.

For the dielectric slab, the author reports that the PBF solution shows excellent agreement with the PWS solution. Kent notes that the reverse surface wave component provides the dominant scattered field $\vec{E}^s$ at near-grazing angles

2.2.3 Hybrid Basis Functions Several attempts have been made to use basis functions that take the form of asymptotic solutions to high-frequency scattering problems. The goal is to reduce the number of unknowns sufficiently so that the method of moments can be applied to electrically large scatterers. This technique seems limited to perfectly electrically conducting (PEC) scatterers

Blue (5) examines a two-dimensional (PEC) strip. He hypothesizes that the strip currents may be well approximated by physical optics in the center of the strip, and by the Geometrical Theory of Diffraction (GTD) near the edges. He thus expands the unknown currents as several physical-optics components and several oppositely-directed diffraction components He allows the PO currents to exist only away from the edges, but allows the GTD currents to exist everywhere on the strip. He then solves for the unknown amplitudes of these components by forcing the total current to satisfy (in a least-squared-error sense) the integral equation at M match points, where M is greater than or equal to the number of unknown coefficients. For a PEC strip that is 200 wavelengths wide, Blue achieves good results with just 17 basis functions and 17 match points.

Another hybrid technique involves using GTD currents where the scatterer is smooth and subdomain pulses near edges and other discontinuities. Burnside (7) analyzes a 2λ PEC square cylinder using 16 pulses at the four corners and eight diffracted currents, for a total of 24 unknowns The unknowns are found using least-squares point matching. The results agree very well with a standard moment methods using straight pulse/point-matching with 56 unknowns.

Thiele and Newhouse (26) modify the generalized impedance matrix to include contributions from GTD currents, with an emphasis on near-field interactions. Specifically, they investigate a monopole on a PEC wedge, a monopole on a PEC circular disc, and a monopole near a PEC step Inclusion of GTD effects allows Thiele and Newhaouse to reduce the size of the impedance matrix

while maintaining good agreement with measured data They suggests that

> .. a potential advantage of such an approach is that in many problems the impedance matrix may be small enough to calculate data at sufficiently many frequencies to obtain time domain solutions via Fourier transformation...

Sahalos and Thiele (23) extend the techniques to three dimensions by analyzing the scattering from a three-sided PEC pyramid After achieving encouraging results, the authors suggest that the GTD-MM technique may be applied to a PEC pyramid with a dielectric coating on one or more faces.

The hybrid techniques are similar to physical basis functions in that both approaches attempt to exploit the expected form of the scattered fields. The two approaches differ in two important respects, however. First, hybrid techniques use functions from the asymptotic high-frequency solutions of GTD and PO while physical basis functions use functions from the corresponding one-dimensional scatterer. Second, hybrid techniques tend to be subsectional in that they use different basis functions over different parts of the scatterer based on proximity to discontinuities. On the other hand, physical basis functions are entire basis functions and exist over the entire scatterer, even near the edges.

2.3 Implications to Problem at Hand

Much work has been done in the analysis of the low-frequency EM scattering from two-dimensional dielectric-coated conducting cylinders of arbitrary cross-section. The standard method is to replace the unknown scattered field $\vec{E}^s$ with unknown equivalent surface and volumetric current densities J and M, write integral equations for J and M, and find approximate solutions to the integral equations using the moment method.

The dielectric-coated conducting strip is a specific case of the dielectric-coated conducting cylinder of arbitrary cross-section. It may be replaced by the equivalent surface and volume current

problem, and integral equations written to relate J and M to the incident field $\vec{E}^i$. We suspect that currents are dominated by the "forced" wave and two surface waves that comprise the physical basis functions, and that a moment method solution using PBFs should yield an accurate solution while minimizing computer time and storage requirements

III. Theory

3.1 Scattering Geometry

Consider a perfectly conducting thin strip of finite width w and infinite length, coated on one side with a material slab of width w and thickness h, as shown in Figure 1. The material is characterized by permeability $\mu_d = \mu_r\mu_0$ and permittivity $\epsilon_d = \epsilon_r\epsilon_0$, where μ_0 and ϵ_0 are the permeability and permittivity of free space, respectively. μ_r and ϵ_r are, in general, complex quantities with real parts greater than unity. If μ_r and ϵ_r are real, then the material is lossless

The time-harmonic incident wave is a transverse-electric (TE) polarized uniform plane wave, with the electric field vector $\vec{\mathbf{E}}$ in the xy-plane and the magnetic field vector $\vec{\mathbf{H}}$ parallel to the z-axis. The time dependence $e^{j\omega t}$ is assumed and suppressed.

3.2 Integral Equations

The total electric and magnetic fields are composed of incident and scattered components

$$\vec{\mathbf{E}}^T = \vec{\mathbf{E}}^i + \vec{\mathbf{E}}^s \qquad [V/m] \tag{1}$$

$$\vec{\mathbf{H}}^T = \vec{\mathbf{H}}^i + \vec{\mathbf{H}}^s \qquad [A/m] \tag{2}$$

We define the incident field ($\vec{\mathbf{E}}^i$ and $\vec{\mathbf{H}}^i$) to be that which *would exist if the scatterer were not present* and the total field ($\vec{\mathbf{E}}^T$ and $\vec{\mathbf{H}}^T$) to be that which *exists in the presence of the scatterer.* The scattered field ($\vec{\mathbf{E}}^s$ and $\vec{\mathbf{H}}^s$) is the thus the difference between the incident and total fields.

All fields must satisfy Maxwell's equations for time-harmonic electromagnetic waves. Additionally, the scattering geometry dictates that certain boundary conditions must be met. The first boundary condition requires the total tangential electric field to vanish at the conductor (8:34), or mathematically, $\hat{\mathbf{n}} \times \vec{\mathbf{E}}^T = 0$ for $|x| < \frac{w}{2}$ and $y = -\frac{h}{2}$, where $\hat{\mathbf{n}}$ is the unit vector normal to the

conductor surface. The second boundary condition requires continuity of the tangential electric and magnetic fields across the material/free-space interface (3:14-15)

3.2.1 Equivalent Currents The surface and volume equivalence theorems (3, 8) allow us to replace the scatterer with free space and equivalent electric and magnetic currents which radiate the scattered fields as shown in Figure 2. A conduction surface current density (8:34)

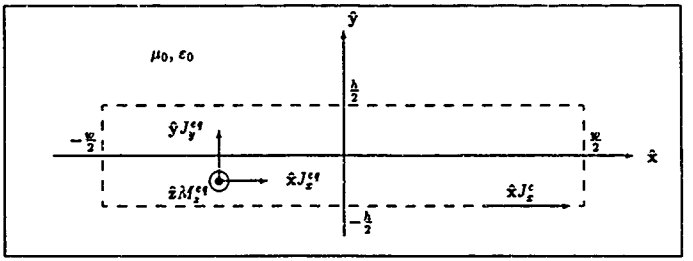

Figure 2. Equivalent Currents

$$\vec{J}^c = \hat{x}J_x^c$$
$$= \hat{n} \times \vec{H}^T = \hat{y} \times \hat{z}H_z^T = \hat{x}H_z^T \qquad [A/m] \tag{3}$$

exists on the conductor ($|x| < \frac{w}{2}, y = -\frac{h}{2}$) while equivalent polarization electric and magnetic current densities (3:328)

$$\vec{J}^{eq} = \hat{x}J_x^{eq} + \hat{y}J_y^{eq}$$
$$= j\omega\epsilon_o(\epsilon_r - 1)\vec{E}^T \qquad [A/m^2] \tag{4}$$
$$\vec{M}^{eq} = \hat{z}M_z^{eq}$$
$$= j\omega\mu_o(\mu_r - 1)\vec{H}^T \qquad [V/m^2] \tag{5}$$

exist within the material ($|x| < \frac{w}{2}, |y| < \frac{h}{2}$) Notice the difference in units between the conduction and equivalent current densities. $\vec{J}^c$, $\vec{J}^{eq}$, and $\vec{M}^{eq}$ radiate the scattered fields $\vec{E}^s$ and $\vec{H}^s$ in free space.

3.2.2 Vector Potentials We may define a magnetic vector potential $\vec{A}$ as the integration of the electric current density $\vec{J}$ against a kernel function (8:80):

$$\vec{A}(\vec{r}) = \iiint \vec{J}(\vec{r}') \frac{e^{-jk_0|\vec{r}-\vec{r}'|}}{4\pi|\vec{r}-\vec{r}'|} dx'\,dy'\,dz' \tag{6}$$

$$\vec{r} = x\hat{x} + y\hat{y} + z\hat{z} \tag{7}$$

$$|\vec{r}-\vec{r}'| = \sqrt{(x-x')^2 + (y-y')^2 + (z-z')^2} \tag{8}$$

$$k_0 = \omega\sqrt{\mu_0\varepsilon_0} \tag{9}$$

The scatterer is two-dimensional, so $\vec{J}$ is not a function of x' (see Eqs 3 and 4) and the integration in x' may be evaluated analytically using the identity (3:581)

$$\int_{-\infty}^{\infty} \frac{e^{-j\alpha\sqrt{x^2+t^2}}}{\sqrt{x^2+t^2}} dt = -j\pi H_0^{(2)}(\alpha x) \tag{10}$$

where $H_0^{(2)}$ is the Hankel function of the second kind of order 0 Furthermore, the currents exist only on the strip and within the material ($|x| \leq \frac{w}{2}$ and $|y| \leq \frac{h}{2}$), so the magnetic vector potential is then

$$\vec{A}(x,y) = \int_{-\frac{h}{2}}^{\frac{h}{2}} \int_{-\frac{w}{2}}^{\frac{w}{2}} \vec{J}(x',y') \frac{1}{4j} H_0^{(2)}\left(k_0\sqrt{(x-x')^2+(y-y')^2}\right) dx'\,dy' \tag{11}$$

The integration kernel

$$\frac{1}{4j} H_0^{(2)}\left(k_0\sqrt{(x-x')^2+(y-y')^2}\right) \tag{12}$$

is the two-dimensional free-space Green's function (3.902), $G(x,y;x',y')$, so we may equivalently write

$$\vec{A}(x,y) = \int_{-\frac{h}{2}}^{\frac{h}{2}} \int_{-\frac{w}{2}}^{\frac{w}{2}} \vec{J}(x',y') G(x,y,x',y')\, dx'\, dy' \tag{13}$$

The electric current density $\vec{J}$ is composed of two parts, the one-dimensional conduction current density $\vec{J}^c$ (Equation 3) and the two-dimensional equivalent polarization current density $\vec{J}^{eq}$ (Equation 4). Thus, by superposition, the magnetic vector potential may be written as the sum of two integrals

$$\begin{aligned} \vec{A}(x,y) &= \int_{-\frac{w}{2}}^{\frac{w}{2}} \vec{J}^c(x') G(x,y;x',-\frac{h}{2})\, dx' \\ &\quad + \int_{-\frac{h}{2}}^{\frac{h}{2}} \int_{-\frac{w}{2}}^{\frac{w}{2}} \vec{J}^{eq}(x',y') G(x,y;x',y')\, dx'\, dy' \end{aligned} \tag{14}$$

Notice that $y' = -\frac{h}{2}$ in the line integral of Equation 14.

By duality (8:98-100), an electric vector potential $\vec{F}$ can be defined as a function of the equivalent magnetic current density $\vec{M} = \vec{M}^{eq}$

$$\vec{F}(x,y) = \int_{-\frac{h}{2}}^{\frac{h}{2}} \int_{-\frac{w}{2}}^{\frac{w}{2}} \vec{M}^{eq}(x',y') G(x,y,x',y')\, dx'\, dy' \tag{15}$$

Notice that there is no one-dimensional magnetic conduction current on the strip.

3 2 3 Scattered Fields in Terms of Vector Potentials The scattered fields ($\vec{E}^s$ and $\vec{H}^s$) are related to the vector potentials ($\vec{A}^s$ and $\vec{F}^s$) and current densities ($\vec{J}$ and $\vec{M}$) by (8:99)

$$\vec{E}^s = -\nabla \times \vec{F} + \frac{1}{j\omega\varepsilon_0}(\nabla \times \nabla \times \vec{A} - \vec{J}) \tag{16}$$

$$\vec{H}^s = \nabla \times \vec{A} + \frac{1}{j\omega\mu_0}(\nabla \times \nabla \times \vec{F} - \vec{M}) \tag{17}$$

Equations 16 and 17 may be simplified by noting that the electric and magnetic vector potentials satisfy the inhomogeneous Helmholtz equations (8:77)

$$\nabla^2 \vec{A} + k_0^2 \vec{A} = -\vec{J} \tag{18}$$

$$\nabla^2 \vec{F} + k_0^2 \vec{F} = -\vec{M} \tag{19}$$

and making use of the vector identity $\nabla \times \nabla \times \vec{\psi} = \nabla(\nabla \cdot \vec{\psi}) - \nabla^2 \vec{\psi}$ (3:927) We may then recast Equations 16 and 17 as

$$\vec{E}^s = -\nabla \times \vec{F} - j\omega\mu_0 \vec{A} + \frac{1}{j\omega\epsilon_0}\nabla(\nabla \cdot \vec{A}) \tag{20}$$

$$\vec{H}^s = \nabla \times \vec{A} - j\omega\epsilon_0 \vec{F} + \frac{1}{j\omega\mu_0}\nabla(\nabla \cdot \vec{F}) \tag{21}$$

To make use of Equations 20 and 21, we will need to define the the gradient of the divergence ($\nabla[\nabla \cdot \vec{\psi}]$) and the curl ($\nabla \times \vec{\psi}$) operators acting on $\vec{A}$ and $\vec{F}$ Noting that $\frac{\partial}{\partial z} = 0$, the elementary operators (gradient, divergence, and curl) acting on arbitrary scalar and vector functions ψ and $\vec{\psi} = \psi_x \hat{x} + \psi_y \hat{y} + \psi_z \hat{z}$, respectively, are given by (3:925)

$$\nabla\psi = \hat{x}\frac{\partial\psi}{\partial x} + \hat{y}\frac{\partial\psi}{\partial y} \tag{22}$$

$$\nabla \cdot \vec{\psi} = \frac{\partial\psi_x}{\partial x} + \frac{\partial\psi_y}{\partial y} \tag{23}$$

$$\nabla \times \vec{\psi} = \hat{x}\frac{\partial\psi_z}{\partial y} - \hat{y}\frac{\partial\psi_z}{\partial x} + \hat{z}\left\{\frac{\partial\psi_y}{\partial x} - \frac{\partial\psi_x}{\partial y}\right\} \tag{24}$$

We construct the gradient of the divergence operator using Equations 22 and 23 as

$$\begin{aligned}\nabla(\nabla \cdot \vec{\psi}) &= \left(\hat{x}\frac{\partial}{\partial x} + \hat{y}\frac{\partial}{\partial y}\right)\left(\frac{\partial\psi_x}{\partial x} + \frac{\partial\psi_y}{\partial y}\right) \\ &= \hat{x}\left\{\frac{\partial^2\psi_x}{\partial x^2} + \frac{\partial^2\psi_y}{\partial x\partial y}\right\} + \hat{y}\left\{\frac{\partial^2\psi_x}{\partial x\partial y} + \frac{\partial^2\psi_y}{\partial y^2}\right\}\end{aligned} \tag{25}$$

3.2.4 Vector Potential in Terms of Current Densities It is convenient to think of the vector potentials as being composed of three components, each radiated by one of the three current densities $\vec{J}^c$, $\vec{J}^{ef}$, or $\vec{M}^{ef}$. Then

$$\begin{aligned}\vec{A}^c(x,y) &= \hat{x}A_x^c(x,y) \\ &= \hat{x}\int_{-\frac{w}{2}}^{\frac{w}{2}} J_x^c(x')\,G(x,y;x',-\tfrac{h}{2})\,dx' \\ \vec{A}^{ef}(x,y) &= \hat{x}A_x^{ef}(x,y) + \hat{y}A_y^{ef}(x,y)\end{aligned} \tag{26}$$

$$= \int_{-\frac{b}{2}}^{\frac{b}{2}} \int_{-\frac{a}{2}}^{\frac{a}{2}} \left\{ \hat{x} J_x^{ef}(x', y') + \hat{y} J_y^{ef}(x', y') \right\} G(x, y, x', y')\, dx'\, dy' \tag{27}$$

$$\vec{F}^{ef}(x, y) = \hat{z} F_z^{ef}(x, y)$$

$$= \hat{z} \int_{-\frac{b}{2}}^{\frac{b}{2}} \int_{-\frac{a}{2}}^{\frac{a}{2}} M_z^{ef}(x', y') G(x, y, x', y')\, dx'\, dy' \tag{28}$$

In Equations 26, 27, and 28, the current densities are functions of primed variables, and the Green's function, G, (see Equation 12) is a function of primed and unprimed coordinates In the following development, the arguments of the current densities and G are suppressed for brevity.

To use Equations 20 and 21, we need the curl and the divergence of the gradient of the three vector potential components. Noting that $A_y^c = A_z^c = A_z^{ef} = F_x^{ef} = F_y^{ef} = 0$ and using Equations 24, 25, 26, 27, and 28, we write

$$\nabla \times \vec{A} = \hat{x} \left\{ \frac{\partial}{\partial y} A_x^c + \frac{\partial}{\partial x} A_y^{ef} - \frac{\partial}{\partial y} A_x^{ef} \right\} \tag{29}$$

$$\nabla \times \vec{F} = \left\{ \hat{x} \frac{\partial}{\partial y} - \hat{y} \frac{\partial}{\partial x} \right\} F_z^{ef} \tag{30}$$

$$\nabla(\nabla \cdot \vec{A}) = \hat{x} \left\{ \frac{\partial^2}{\partial x^2} A_x^c + \frac{\partial^2}{\partial x^2} A_x^{ef} + \frac{\partial^2}{\partial x \partial y} A_y^{ef} \right\} + \hat{y} \left\{ \frac{\partial^2}{\partial x \partial y} A_x^c + \frac{\partial^2}{\partial x \partial y} A_x^{ef} + \frac{\partial^2}{\partial y^2} A_y^{ef} \right\} \tag{31}$$

$$\nabla(\nabla \cdot \vec{F}) = 0 \tag{32}$$

We may now substitute Equations 26, 27,and 28 into Equations 29–32 to yield

$$\nabla \times \vec{A} = \hat{x} \left\{ -\frac{\partial}{\partial y} \int_{-\frac{a}{2}}^{\frac{a}{2}} J_x^c G\, dx' + \frac{\partial}{\partial x} \int_{-\frac{b}{2}}^{\frac{b}{2}} \int_{-\frac{a}{2}}^{\frac{a}{2}} J_y^{ef} G\, dx'\, dy' - \frac{\partial}{\partial y} \int_{-\frac{b}{2}}^{\frac{b}{2}} \int_{-\frac{a}{2}}^{\frac{a}{2}} J_x^{ef} G\, dx'\, dy' \right\} \tag{33}$$

$$\nabla \times \vec{F} = \left\{ \hat{x} \frac{\partial}{\partial y} - \hat{y} \frac{\partial}{\partial x} \right\} \int_{-\frac{a}{2}}^{\frac{a}{2}} \int_{-\frac{b}{2}}^{\frac{b}{2}} M_z^{ef} G\, dx'\, dy' \tag{34}$$

$$\nabla(\nabla \cdot \vec{A}) = \hat{x} \left\{ \frac{\partial^2}{\partial x^2} \int_{-\frac{a}{2}}^{\frac{a}{2}} J_x^c G\, dx' + \frac{\partial^2}{\partial x^2} \int_{-\frac{b}{2}}^{\frac{b}{2}} \int_{-\frac{a}{2}}^{\frac{a}{2}} J_x^{ef} G\, dx'\, dy' + \frac{\partial^2}{\partial x \partial y} \int_{-\frac{b}{2}}^{\frac{b}{2}} \int_{-\frac{a}{2}}^{\frac{a}{2}} J_y^{ef} G\, dx'\, dy' \right\}$$

$$+\hat{y}\left\{\frac{\partial^2}{\partial x\partial y}\int_{-\frac{w}{2}}^{\frac{w}{2}} J_x^c G\,dx' + \frac{\partial^2}{\partial x\partial y}\int_{-\frac{w}{2}}^{\frac{w}{2}}\int_{-\frac{h}{2}}^{\frac{h}{2}} J_x^{ef} G\,dx'dy' + \frac{\partial^2}{\partial y^2}\int_{-\frac{w}{2}}^{\frac{w}{2}}\int_{-\frac{h}{2}}^{\frac{h}{2}} J_y^{ef} G\,dx'dy'\right\} \quad (35)$$

$$\nabla(\nabla\cdot\vec{F}) = 0 \quad (36)$$

3.2.5 The Scattered Fields Equations 33–36 can be decomposed into parts associated with J_x^c, J_x^{ef}, J_y^{ef}, and M_x^{ef}. We can then find the scattered electric field $\vec{E}^s$ as a function of J_x^c, J_x^{ef}, J_y^{ef}, and M_x^{ef} using Equations 20, 34, 14, and 35. This gives

$$\vec{E}^s = \vec{E}^s(J_x^c) + \vec{E}^s(J_x^{ef}) + \vec{E}^s(J_y^{ef}) + \vec{E}^s(M_x^{ef}) \quad (37)$$

$$\vec{E}^s(J_x^c) = -j\omega\mu_0\hat{x}\int_{-\frac{w}{2}}^{\frac{w}{2}} J_x^c G\,dx' + \frac{1}{j\omega\varepsilon_0}\left\{\hat{x}\frac{\partial^2}{\partial x^2}\int_{-\frac{w}{2}}^{\frac{w}{2}} J_x^c G\,dx' + \hat{y}\frac{\partial^2}{\partial x\partial y}\int_{-\frac{w}{2}}^{\frac{w}{2}} J_x^c G\,dx'\right\} \quad (38)$$

$$\vec{E}^s(J_x^{ef}) = -j\omega\mu_0\hat{x}\int_{-\frac{h}{2}}^{\frac{h}{2}}\int_{-\frac{w}{2}}^{\frac{w}{2}} J_x^{ef} G\,dx'dy' + \frac{1}{j\omega\varepsilon_0}\left\{\hat{x}\frac{\partial^2}{\partial x^2}\int_{-\frac{h}{2}}^{\frac{h}{2}}\int_{-\frac{w}{2}}^{\frac{w}{2}} J_x^{ef} G\,dx'dy' + \hat{y}\frac{\partial^2}{\partial x\partial y}\int_{-\frac{h}{2}}^{\frac{h}{2}}\int_{-\frac{w}{2}}^{\frac{w}{2}} J_x^{ef} G\,dx'dy'\right\} \quad (39)$$

$$\vec{E}^s(J_y^{ef}) = -j\omega\mu_0\hat{y}\int_{-\frac{w}{2}}^{\frac{w}{2}}\int_{-\frac{h}{2}}^{\frac{h}{2}} J_y^{ef} G\,dx'dy' + \frac{1}{j\omega\varepsilon_0}\left\{\hat{x}\frac{\partial^2}{\partial x\partial y}\int_{-\frac{h}{2}}^{\frac{h}{2}}\int_{-\frac{w}{2}}^{\frac{w}{2}} J_y^{ef} G\,dx'dy' + \hat{y}\frac{\partial^2}{\partial y^2}\int_{-\frac{h}{2}}^{\frac{h}{2}}\int_{-\frac{w}{2}}^{\frac{w}{2}} J_y^{ef} G\,dx'dy'\right\} \quad (40)$$

$$\vec{E}^s(M_x^{ef}) = -\hat{x}\frac{\partial}{\partial y}\int_{-\frac{h}{2}}^{\frac{h}{2}}\int_{-\frac{w}{2}}^{\frac{w}{2}} M_x^{ef} G\,dx'dy' + \hat{y}\frac{\partial}{\partial x}\int_{-\frac{h}{2}}^{\frac{h}{2}}\int_{-\frac{w}{2}}^{\frac{w}{2}} M_x^{ef} G\,dx'dy' \quad (41)$$

(42)

Equivalent expressions for the scattered magnetic field $\vec{H}^s$ are considerably simpler since $\nabla(\nabla\cdot\vec{F}) = 0$, and may be found using Equations 21, 33, 15, and 36

$$\vec{H}^s(J_x^c) = -\hat{z}\frac{\partial}{\partial y}\int_{-\frac{w}{2}}^{\frac{w}{2}} J_x^c G\,dx' \quad (43)$$

$$\vec{H}^s(J_x^{ef}) = -\hat{z}\frac{\partial}{\partial y}\int_{-\frac{h}{2}}^{\frac{h}{2}}\int_{-\frac{w}{2}}^{\frac{w}{2}} J_x^{ef} G\,dx'dy' \quad (44)$$

$$\vec{H}^s(J_y^{eq}) = \hat{z}\frac{\partial}{\partial x}\int_{-\frac{b}{2}}^{\frac{b}{2}}\int_{-\frac{w}{2}}^{\frac{w}{2}} J_y^{eq}\, G\, dx'\, dy' \tag{45}$$

$$\vec{H}^s(M_z^{eq}) = -j\omega\varepsilon_0\hat{z}\int_{-\frac{b}{2}}^{\frac{b}{2}}\int_{-\frac{w}{2}}^{\frac{w}{2}} M_z^{eq}\, G\, dx'\, dy' \tag{46}$$

We can restructure Equations 38–41 to find the x and y components of $\vec{E}^s$ Noting that $k_0^2 = \omega^2\mu_0\varepsilon_0$, we find

$$\vec{E}^s = \hat{x}E_x^s + \hat{y}E_y^s \tag{47}$$

$$E_x^s(J_x^c) = \frac{1}{j\omega\varepsilon_0}\left\{k_0^2 + \frac{\partial^2}{\partial x^2}\right\}\int_{-\frac{w}{2}}^{\frac{w}{2}} J_x^c\, G\, dx' \tag{48}$$

$$E_x^s(J_x^{eq}) = \frac{1}{j\omega\varepsilon_0}\left\{k_0^2 + \frac{\partial^2}{\partial x^2}\right\}\int_{-\frac{b}{2}}^{\frac{b}{2}}\int_{-\frac{w}{2}}^{\frac{w}{2}} J_x^{eq}\, G\, dx'\, dy' \tag{49}$$

$$E_x^s(J_y^{eq}) = \frac{1}{j\omega\varepsilon_0}\frac{\partial^2}{\partial x\partial y}\int_{-\frac{b}{2}}^{\frac{b}{2}}\int_{-\frac{w}{2}}^{\frac{w}{2}} J_y^{eq}\, G\, dx'\, dy' \tag{50}$$

$$E_x^s(M_z^{eq}) = -\frac{\partial}{\partial y}\int_{-\frac{b}{2}}^{\frac{b}{2}}\int_{-\frac{w}{2}}^{\frac{w}{2}} M_z^{eq}\, G\, dx'\, dy' \tag{51}$$

$$E_y^s(J_x^c) = \frac{1}{j\omega\varepsilon_0}\frac{\partial^2}{\partial x\partial y}\int_{-\frac{w}{2}}^{\frac{w}{2}} J_x^c\, G\, dx' \tag{52}$$

$$E_y^s(J_x^{eq}) = \frac{1}{j\omega\varepsilon_0}\frac{\partial^2}{\partial x\partial y}\int_{-\frac{b}{2}}^{\frac{b}{2}}\int_{-\frac{w}{2}}^{\frac{w}{2}} J_x^{eq}\, G\, dx'\, dy' \tag{53}$$

$$E_y^s(J_y^{eq}) = \frac{1}{j\omega\varepsilon_0}\left\{k_0^2 + \frac{\partial^2}{\partial y^2}\right\}\int_{-\frac{b}{2}}^{\frac{b}{2}}\int_{-\frac{w}{2}}^{\frac{w}{2}} J_y^{eq}\, G\, dx'\, dy' \tag{54}$$

$$E_y^s(M_z^{eq}) = \frac{\partial}{\partial x}\int_{-\frac{b}{2}}^{\frac{b}{2}}\int_{-\frac{w}{2}}^{\frac{w}{2}} M_z^{eq}\, G\, dx'\, dy' \tag{55}$$

3.2.6 The Final Integral Equations The material coating of interest in this thesis is a non-magnetic dielectric. Then $\mu_r = 1$ and by Equation 5 no equivalent magnetic current $\vec{M}$ exists and the scattered fields are given by Equations 43–45 (for H_z^s), 48–50 (for E_x^s), and 52–54 (for E_y^s) We now wish to write a set of integral equations in which the only unknowns are the current densities

$\vec{J}^{eq}$ and $\vec{J}^{c}$. This set is

$$E_x^s = \frac{1}{j\omega\varepsilon_0(\varepsilon_r-1)}J_x^{eq} - \frac{1}{j\omega\varepsilon_0}\left\{\left[k_0^2+\frac{\partial^2}{\partial x^2}\right]\int_{-\frac{b}{2}}^{\frac{b}{2}}\int_{-\frac{w}{2}}^{\frac{w}{2}} J_x^{eq}\,G\,dx'\,dy' + \frac{\partial^2}{\partial x\partial y}\int_{-\frac{b}{2}}^{\frac{b}{2}}\int_{-\frac{w}{2}}^{\frac{w}{2}} J_y^{eq}\,G\,dx'\,dy' + \left[k_0^2+\frac{\partial^2}{\partial x^2}\right]\int_{-\frac{w}{2}}^{\frac{w}{2}} J_x^{c}\,G\,dx'\right\} \quad (56)$$

$$E_y^s = \frac{1}{j\omega\varepsilon_0(\varepsilon_r-1)}J_y^{eq} - \frac{1}{j\omega\varepsilon_0}\left\{\frac{\partial^2}{\partial x\partial y}\int_{-\frac{b}{2}}^{\frac{b}{2}}\int_{-\frac{w}{2}}^{\frac{w}{2}} J_x^{eq}\,G\,dx'\,dy' + \left[k_0^2+\frac{\partial^2}{\partial y^2}\right]\int_{-\frac{b}{2}}^{\frac{b}{2}}\int_{-\frac{w}{2}}^{\frac{w}{2}} J_y^{eq}\,G\,dx'\,dy' + \frac{\partial^2}{\partial x\partial y}\int_{-\frac{w}{2}}^{\frac{w}{2}} J_x^{c}\,G\,dx'\right\} \quad (57)$$

$$H_z^s = H_z^T + \frac{\partial}{\partial y}\int_{-\frac{b}{2}}^{\frac{b}{2}}\int_{-\frac{w}{2}}^{\frac{w}{2}} J_x^{eq}\,G\,dx'\,dy' - \frac{\partial}{\partial x}\int_{-\frac{b}{2}}^{\frac{b}{2}}\int_{-\frac{w}{2}}^{\frac{w}{2}} J_y^{eq}\,G\,dx'\,dy' + \frac{\partial}{\partial y}\int_{-\frac{w}{2}}^{\frac{w}{2}} J_x^{c}\,G\,dx' \quad (58)$$

Equations 56–58 are three coupled integral equations with unknown quantities J_x^{eq}, J_y^{eq}, and J_x^{c}, and agree with Kent's development (15). In Chapter IV, we apply the method of moments to find the unknown currents.

3.3 Two-Dimensional Scattering Width

We are interested in finding the two-dimensional scattering width σ_{2D} of the dielectric-coated conducting strip, both monostatically (in the direction of the incident wave) and bistatically (not in the direction of the incident wave), as shown in Figure 3 The scattering width is given by (3.577)

$$\sigma_{2D} = \lim_{\rho\to\infty}\left[2\pi\rho\frac{|\vec{E}^s|^2}{|\vec{E}^i|^2}\right] \quad (59)$$

If we let the incident plane wave have unit amplitude, $|\vec{E}^i| = 1$, then Equation 59 becomes simply

$$\sigma_{2D} = \lim_{\rho\to\infty} 2\pi\rho|\vec{E}^s|^2 \quad (60)$$

Using Equations 47–55, and assuming the observation point (x, y) lies outside the scatterer, we may move the derivatives inside the integrals (This is valid since the singularity of the Green's

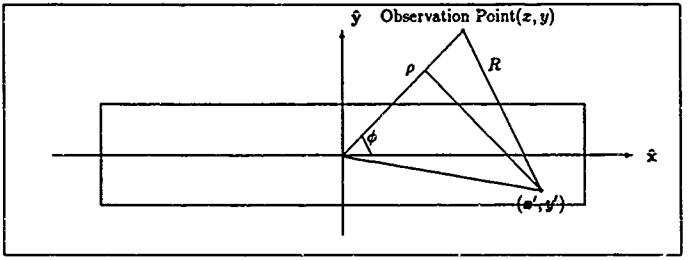

Figure 3 The Scattered Field

function is not in the region of integration.) Substituting expressions for $\frac{\partial^2 G}{\partial x^2}$, $\frac{\partial^2 G}{\partial x \partial y}$, and $\frac{\partial^2 G}{\partial y^2}$ (see Appendix E), we find the scattered electric field is given by

$$\begin{aligned} E_x^s(x,y) &= \frac{-\omega\mu_0}{4}\left\{\int_{-\frac{w}{2}}^{\frac{w}{2}} J_x^c(x')\left[\frac{H_1^{(2)}(k_0R)}{k_0R} - \frac{(y+\frac{h}{2})^2}{R^2}H_2^{(2)}(k_0R)\right]dx'\right. \\ &\quad + \int_{\frac{h}{2}}^{\frac{h}{2}}\int_{-\frac{w}{2}}^{\frac{w}{2}} J_x^{cq}(x',y')\left[\frac{H_1^{(2)}(k_0R)}{k_0R} - \frac{(y-y')^2}{R^2}H_2^{(2)}(k_0R)\right]dx'\,dy' \\ &\quad \left. + \int_{\frac{h}{2}}^{\frac{h}{2}}\int_{-\frac{w}{2}}^{\frac{w}{2}} J_y^{cq}(x',y')\frac{(x-x')(y-y')}{R^2}H_2^{(2)}(k_0R)\,dx'\,dy'\right\} \qquad (61) \\ E_y^s(x,y) &= \frac{-\omega\mu_0}{4}\left\{\int_{-\frac{w}{2}}^{\frac{w}{2}} J_x^c(x')\frac{(x-x')(y+\frac{h}{2})}{R^2}H_2^{(2)}(k_0R)\,dx'\right. \\ &\quad + \int_{\frac{h}{2}}^{\frac{h}{2}}\int_{-\frac{w}{2}}^{\frac{w}{2}} J_x^{cq}(x',y')\frac{(x-x')(y-y')}{R^2}H_2^{(2)}(k_0R)\,dx'\,dy' \\ &\quad \left. + \int_{\frac{h}{2}}^{\frac{h}{2}}\int_{-\frac{w}{2}}^{\frac{w}{2}} J_y^{cq}(x',y')\left[\frac{H_1^{(2)}(k_0R)}{k_0R} - \frac{(x-x')^2}{R^2}H_2^{(2)}(k_0R)\right]dx'\,dy'\right\} \qquad (62) \end{aligned}$$

where $R = \sqrt{(x-x')^2 + (y-y')^2}$.

We are interested in the scattered field far from the scatterer, i.e., in the limit as $\rho \to \infty$. We may then replace the Hankel functions by their large-argument asymptotic forms (17.364). For amplitude terms, we may replace R with ρ, $(x-x')$ with $\rho\cos\phi$, and $(y-y')$ with $\rho\sin\phi$. For phase terms, we may replace R with $\rho - x'\cos\phi - y'\sin\phi$. We also see that as $\rho \to \infty$, the terms containing $H_1^{(2)}(k_0R)$ become subdominant to terms containing $H_2^{(2)}(k_0R)$ and may be neglected

We may then write

$$E_x^s(x,y) = \frac{\omega\mu_0}{4}\sqrt{\frac{2}{\pi k_0 \rho}}\, e^{-j(k_0\rho - 5\pi/4)} \sin\phi\, I \tag{63}$$

$$E_y^s(x,y) = \frac{-\omega\mu_0}{4}\sqrt{\frac{2}{\pi k_0 \rho}}\, e^{-j(k_0\rho - 5\pi/4)} \cos\phi\, I \tag{64}$$

$$\begin{aligned} I = \Bigg\{ & \sin\phi \int_{-\frac{\pi}{2}}^{\frac{\pi}{2}} J_x^c(x',y')\, e^{jk_0(x'\cos\phi - \frac{h}{2}\sin\phi)} dx' \\ & + \sin\phi \int_{-\frac{\pi}{2}}^{\frac{\pi}{2}} \int_{-\frac{h}{2}}^{\frac{h}{2}} J_x^{cf}(x',y')\, e^{jk_0(x'\cos\phi + y'\sin\phi)} dx'\, dy' \\ & - \cos\phi \int_{-\frac{\pi}{2}}^{\frac{\pi}{2}} \int_{-\frac{h}{2}}^{\frac{h}{2}} J_y^{cf}(x',y')\, e^{jk_0(x'\cos\phi + y'\sin\phi)} dx'\, dy' \Bigg\} \end{aligned} \tag{65}$$

If we express the scattered electric field in cylindrical coordinates (3 922), we find

$$E_\rho^s = \cos\phi\, E_x^s + \sin\phi\, E_y^s = 0 \tag{66}$$

$$\begin{aligned} E_\phi^s &= -\sin\phi\, E_x^s + \cos\phi\, E_y^s \\ &= \frac{-\omega\mu_0}{4}\sqrt{\frac{2}{\pi k_0 \rho}}\, e^{-j(k_0\rho - 5\pi/4)}\, I \end{aligned} \tag{67}$$

As expected, the scattered field has no radial component in the far field

Plugging Equation 67 into Equation 60, we now write the two-dimensional scattering width as

$$\sigma_{2D} = \frac{\omega\mu_0\eta_0}{4}\,|I|^2 \tag{68}$$

Once the currents J_x^c, J_x^{cf}, and J_y^{cf} are found, Equations 65 and 68 may be used to find the scattering width of the dielectric-coated conducting strip for any observation angle ϕ.

IV. Moment Method Solution Using Physical Basis Functions

Equations 56–58 define the unknown current densities J_x^{sf}, J_y^{sf}, and J_x^c in terms of the known incident field components E_z^i, E_y^i, and H_z^i. Unfortunately, these integral equations cannot be solved analytically. We apply the method of moments (9) and transform the integral equations into a set of linear algebraic equations which can be solved numerically.

4.1 Basis Functions

The first step in the method of moments is to select a set of basis functions in which to expand the unknown quantities.

$$J_x^{sf}(x,y) = \sum_{n=1}^{N} a_n f_n^a(x,y) \tag{69}$$

$$J_y^{sf}(x,y) = \sum_{n=1}^{N} b_n f_n^b(x,y) \tag{70}$$

$$J_x^c(x,y) = \sum_{n=1}^{N} c_n f_n^c(x,y) \tag{71}$$

We choose to use "physical basis functions" as defined by Richmond (19, 20) and Kent (14) The physical basis functions consist of a "forced" wave and two oppositely-directed surface waves (25) The forced wave is the field that would exist in the dielectric if it were infinitely wide ($w \to \infty$) The surface waves are the dominant zero-order TM^z surface waves which have a cutoff frequency of zero. The forced wave and surface waves are developed in detail in Appendix A In terms of the three physical basis functions, the field and current components in the dielectric may be written as

$$E_z^T(x,y) = \frac{J_z^{sf}(x,y)}{j\omega\epsilon_o(\epsilon_r - 1)} = \sum_{n=1}^{3} A_n c_{zn} \sin\left[f_n\left(y + \frac{h}{2}\right)\right] e^{-j\beta_n z} \tag{72}$$

$$E_y^T(x,y) = \frac{J_y^{sf}(x,y)}{j\omega\epsilon_o(\epsilon_r - 1)} = \sum_{n=1}^{3} A_n c_{yn} \cos\left[f_n\left(y + \frac{h}{2}\right)\right] e^{-j\beta_n z} \tag{73}$$

$$H_x^T(x,y) = \sum_{n=1}^{3} A_n c_{xn} \cos\left[f_n\left(y + \frac{h}{2}\right)\right] e^{-j\beta_n z} \tag{74}$$

$$J_x^c(x) = H_z^T\left(x, -\frac{h}{2}\right) = \sum_{n=1}^{3} A_n\, c_{zn}\, e^{-j g_n x} \tag{75}$$

The terms A_n describe the amplitudes of the physical basis functions relative to each other The "field amplitudes" c_{xn}, c_{yn}, and c_{zn} describe the relative amplitudes of the individual field components of the physical basis functions. The field amplitudes are defined by the form of the physical basis functions; they are developed in Appendix A and given by

$$\begin{bmatrix} c_{x1} & c_{x2} & c_{x3} \\ c_{y1} & c_{y2} & c_{y3} \\ c_{z1} & c_{z2} & c_{z3} \end{bmatrix} = \begin{bmatrix} j\cos\theta_d & \frac{f_2}{j\omega\epsilon_d} & \frac{f_3}{j\omega\epsilon_d} \\ \sin\theta_d & \frac{-g_2}{\omega\epsilon_d} & \frac{-g_3}{\omega\epsilon_d} \\ \sqrt{\epsilon_r}/\eta_o & -1 & -1 \end{bmatrix} \tag{76}$$

An important property of the physical basis functions, and one that sets them apart from pulse bases, piecewise-sinusoids, etc., is that they serve to couple the $x-$, $y-$ and $z-$directed field components Because the physical basis functions individually satisfy Maxwell's equations, if we know E_x^T then we automatically know E_y^T and H_z^T. So instead of needing to solve for the $3N$ unknowns of Equations 69- 71 ($a_1, a_2, \ldots, c_N$), we need only solve for the three wave amplitudes A_n.

Propagation constants f_n and g_n are chosen such that $n = 1$ represents the forced wave, $n = 2$ represents the $+x$-directed surface wave, and $n = 3$ represents the $-x$-directed surface wave f_n and g_n are real and functions of the relative permittivity ϵ_r and thickness h of the dielectric, and the angle of incidence θ and frequency ω of the incident wave. Specific equations for f_n and g_n are given in Appendix A; in this chapter they are treated as known constants.

Expanding the currents in Equations 56-58, we find

$$\begin{aligned} E_x^i(x,y) \;=\; & \sum_{n=1}^{3} A_n\, c_{xn} \sin\left[f_n\left(y+\frac{h}{2}\right)\right] e^{-j g_n x} \\ & - (\epsilon_r - 1)\left[k_o^2 + \frac{\partial^2}{\partial x^2}\right] \iint_S \sum_{n=1}^{3} A_n\, c_{xn} \sin\left[f_n\left(y'+\frac{h}{2}\right)\right] e^{-j g_n x'} G\, dx'\, dy' \\ & - (\epsilon_r - 1)\frac{\partial^2}{\partial x \partial y} \iint_S \sum_{n=1}^{3} A_n\, c_{yn} \cos\left[f_n\left(y'+\frac{h}{2}\right)\right] e^{-j g_n x'} G\, dx'\, dy' \end{aligned}$$

$$- \frac{1}{j\omega\varepsilon_o}\left[k_o^2 + \frac{\partial^2}{\partial x^2}\right]\int_C \sum_{n=1}^{3} A_n c_{zn} e^{-j\beta_n x'} G\, dx' \tag{77}$$

$$\begin{aligned} E_y^s(x,y) \;=\; & \sum_{n=1}^{3} A_n c_{yn} \cos\left[f_n\left(y+\frac{h}{2}\right)\right] e^{-j\beta_n x} \\ & - (\varepsilon_r - 1)\frac{\partial^2}{\partial x \partial y}\iint_S \sum_{n=1}^{3} A_n c_{zn} \sin\left[f_n\left(y'+\frac{h}{2}\right)\right] e^{-j\beta_n x'} G\, dx'\, dy' \\ & - (\varepsilon_r - 1)\left[k_o^2 + \frac{\partial^2}{\partial y^2}\right]\iint_S \sum_{n=1}^{3} A_n c_{yn} \cos\left[f_n\left(y'+\frac{h}{2}\right)\right] e^{-j\beta_n x'} G\, dx'\, dy' \\ & - \frac{1}{j\omega\varepsilon_o}\frac{\partial^2}{\partial x \partial y}\int_C \sum_{n=1}^{3} A_n c_{zn} e^{-j\beta_n x'} G\, dx' \end{aligned} \tag{78}$$

$$\begin{aligned} H_x^s(x,y) \;=\; & \sum_{n=1}^{3} A_n c_{zn} \cos\left[f_n\left(y+\frac{h}{2}\right)\right] e^{-j\beta_n x} \\ & \frac{\partial}{\partial y}\iint_S \sum_{n=1}^{3} A_n c_{zn} \sin\left[f_n\left(y'+\frac{h}{2}\right)\right] e^{-j\beta_n x'} G\, dx'\, dy' \\ & -\frac{\partial}{\partial x}\iint_S \sum_{n=1}^{3} A_n c_{yn} \cos\left[f_n\left(y'+\frac{h}{2}\right)\right] e^{-j\beta_n x'} G\, dx'\, dy' \\ & +\frac{\partial}{\partial y}\int_C \sum_{n=1}^{3} A_n c_{zn} e^{-j\beta_n x'} G\, dx' \end{aligned} \tag{79}$$

where $G = \frac{1}{4j} H_0^{(2)}(k_o\sqrt{(x-x')^2+(y-y')^2})$, region S is the cross-sectional area of the dielectric slab ($|x'| \le \frac{w}{2}, |y'| \le \frac{h}{2}$) and contour C lies along the conducting strip ($|x'| \le \frac{w}{2}, y' = -\frac{h}{2}$)

4.2 Testing Functions and Match Points

In order to obtain a system of linear equations to solve for the three unknown wave amplitudes, we must define a set of testing functions. We choose to use M (where $M > 3$) Dirac delta functions which "fire" at the points $\{(x,y)_m\}_{m=1}^{M}$ as the testing functions; this is sometimes referred to as "point matching" where the points $(x,y)_m$ are called "match points" This is equivalent to enforcing, in a least-squares sense, $\vec{E}^T(x,y)_m \simeq \vec{E}^i(x,y)_m + \vec{E}^s(x,y)_m$, $m = 1, M$.

The M match points may lie either on the conductor or within the dielectric slab. No guidelines exist to tell us where to place the match points, so we must write the moment method algorithms to allow many different configurations of match points and then look for convergence

to a common solution. However, we must enforce some order in the match point location, so we partition the dielectric slab into a grid of rectangles, as shown in Figure 4, with each rectangle of size $\Delta x \times \Delta y$. We pick $\Delta x, \Delta y \approx \lambda_d = \sqrt{\varepsilon_r}\lambda_0$ such that an integral number of rectangular cells will fit inside the dielectric. Then we may write

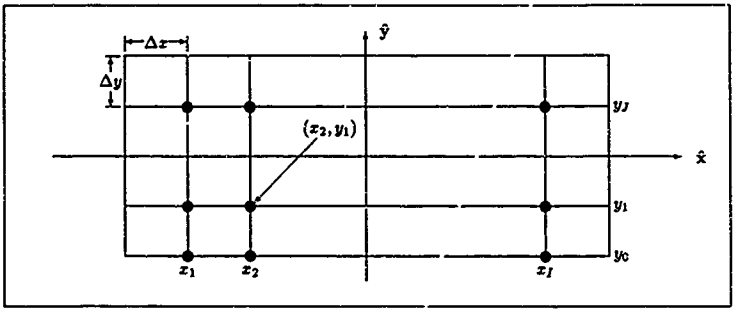

Figure 4. Match Point Locations Within Dielectric Slab

$$w = (I+1)\Delta x \tag{80}$$

$$h = (J+1)\Delta y \tag{81}$$

We then pick $I \times J$ match points in the interior of the dielectric and I match points on the conductor, for a total of $M = I(J+1)$ match points. We may then codify the location of the m^{th} match point as

$$(x,y)_m = (x_i, y_j) \tag{82}$$

where

$$x_i = -\frac{w}{2} + i\Delta x, \qquad i = 1, I \tag{83}$$

$$y_j = -\frac{h}{2} + j\Delta y, \qquad j = 0, J \tag{84}$$

$$m = (i-1)(J+1) + j + 1 \tag{85}$$

For example, if $J = 2$ and $I = 4$, then there are $M = 4 \times (2+1) = 12$ match points, and the fifth match point is given by $(x,y)_5 = (x_2, y_1) = (-\frac{w}{2} + 2\Delta x, -\frac{h}{2} + \Delta y)$.

4.3 System of Linear Equations

The systems of linear equations given by Equations 77– 79 may be written in matrix form as

$$V^{x,y,z} = Z^{x,y,z} I \tag{86}$$

The voltage matrix $V^{x,y,z}$ is a $M \times 1$ vector whose elements are defined by

$$\begin{aligned} V_m^x &= E_x^i(x,y)_m \\ V_m^y &= E_y^i(x,y)_m \qquad\qquad m = 1, M \\ V_m^z &= H_z^i(x,y)_m \end{aligned} \tag{87}$$

The current matrix I is a 3×1 vector composed of the unknown wave amplitudes defined by $\{I_n = A_n\}_{n=1}^3$. The impedance matrix $Z^{x,y,z}$ is a $M \times 3$ matrix whose elements are defined by

$$\begin{aligned} Z_{mn}^x &= c_{xn} \sin\left[f_n\left(y_j + \frac{h}{2}\right)\right] e^{-j g_m x_i} - \\ &\quad \left\{(\epsilon_r - 1)\left[k_o^2 + \frac{\partial^2}{\partial x^2}\right] \iint_S c_{xn} \sin\left[f_n\left(y' + \frac{h}{2}\right)\right] e^{-j g_m x'} G\, dx'\, dy' \right. \\ &\quad + (\epsilon_r - 1) \frac{\partial^2}{\partial x \partial y} \iint_S c_{yn} \cos\left[f_n\left(y' + \frac{h}{2}\right)\right] e^{-j g_m x'} G\, dx'\, dy' \\ &\quad \left. + \frac{1}{j\omega\epsilon_o}\left[k_o^2 + \frac{\partial^2}{\partial x^2}\right] \int_C c_{xn} \cos\left[f_n\left(y' + \frac{h}{2}\right)\right] e^{-j g_m x'} G\, dx' \right\}_{(x,y)=(x_i,y_j)} \end{aligned} \tag{88}$$

$$\begin{aligned} Z_{mn}^y &= c_{yn} \cos\left[f_n\left(y_j + \frac{h}{2}\right)\right] e^{-j g_m x_i} - \\ &\quad \left\{(\epsilon_r - 1) \frac{\partial^2}{\partial x \partial y} \iint_S c_{xn} \sin\left[f_n\left(y' + \frac{h}{2}\right)\right] e^{-j g_m x'} G\, dx'\, dy' \right. \\ &\quad + (\epsilon_r - 1)\left[k_o^2 + \frac{\partial^2}{\partial y^2}\right] \iint_S c_{yn} \cos\left[f_n\left(y' + \frac{h}{2}\right)\right] e^{-j g_m x'} G\, dx'\, dy' \\ &\quad \left. + \frac{1}{j\omega\epsilon_o} \frac{\partial^2}{\partial x \partial y} \int_C c_{xn} \cos\left[f_n\left(y' + \frac{h}{2}\right)\right] e^{-j g_m x'} G\, dx' \right\}_{(x,y)=(x_i,y_j)} \end{aligned} \tag{89}$$

$$\begin{aligned} Z_{mn}^z &= c_{zn} \cos\left[f_n\left(y_j + \frac{h}{2}\right)\right] e^{-j g_m x_i} + \\ &\quad \left\{j\omega\epsilon_0(\epsilon_r - 1) c_{xn} \frac{\partial}{\partial y} \iint_S \sin\left[f_n\left(y' + \frac{h}{2}\right)\right] e^{-j g_m x'} G\, dx'\, dy' \right. \end{aligned}$$

$$-j\omega\varepsilon_0(\epsilon_r-1)c_{yn}\frac{\partial}{\partial x}\iint_S \cos\left[f_n\left(y'+\frac{h}{2}\right)\right]e^{-jf_n x'}G\,dx'\,dy'$$
$$+c_{xn}\frac{\partial}{\partial y}\int_C e^{-jf_n x'}G\,dx'\Bigg\}_{(x,y)=(x_i,y_j)} \tag{90}$$

A conventional moment method solution generates a square impedance matrix, and the unknown vector I is found by inverting the impedance matrix Z. Here, however, we have a non-square impedance matrix, indicating an overdetermined system of equations (This is analogous to the problem of finding a "best fit" line given more than two points in a plane.) As suggested by Sarkar (24), we will solve for I in a least-squared-error sense by multiplying the matrix equations by the conjugate transpose of Z, Z^{*T}, yielding

$$Z^{*T}V = Z^{*T}ZI \tag{91}$$

$Z^{*T}Z$ is a 3 × 3 matrix which can be inverted (if non-singular) and I is given by

$$[Z^{*T}Z]^{-1}Z^{*T}V = I \tag{92}$$

The "goodness of fit" of the solution is determined by the residual r, given by

$$r = V - ZI \tag{93}$$

We may define an error metric as the average relative error, which is given by

$$\text{AvgRelError} = \frac{1}{M}\sum_{m=1}^{M}\left|\frac{r_m}{V_m}\right| \tag{94}$$

4.4 Impedance Matrix $Z^{x,y,z}$

The elements of $Z^{x,y,z}$ are given by Equations 88–90. Unfortunately, all of the surface integrands are singular at the match point $(x,y)_m$ and must be integrated with great care. Additionally, the integrands are functions of x and y, which create problems when we attempt to differentiate them.

The solution is to first define a region S_{1m} (where the subscript m indicates dependence on match point location) about the singular match point such that the integrands in region $S-S_{1m}$ are not affected by the singularity.

Then we can exploit symmetry and small-argument polynomial expansions to analytically evaluate integrals in region S_{1m} and numerically integrate in region $S-S_{1m}$.

Second, Barksdale (4) suggests the change of variables $u = x'-x$ and $v = y'-y$ to move the singular match point to the origin, allowing us to move the x and y dependence out of the integrand. While the limits of integration are still functions of x and y, this dependence is moved from the inner region to the outer region; instead of integrating over regions $S-S_{1m}$ and S_{1m} in xy-coordinates, we now integrate over regions $\tilde{S}_m-\tilde{S}_1$ and $\tilde{S}_1$ in uv-coordinates

A more complete and detailed development of impedance matrices $Z^{x,y,z}$, as well as their rather complicated form, is presented in Appendix B.

4.5 Two-Dimensional Scattering Width

Once the amplitudes of the three physical basis functions are found, we know the equivalent polarization and conduction currents and can use Equations 68 and 65 to find the bistatic two-dimensional scattering width σ_{2D} as a function of the observation angle phi, as depicted in Figure 3

The form of the current expressions, given by Equations 72-75, allows us to evaluate the integrals of Equation 65 analytically (the evaluations are very simple), so that σ_{2D} is proportional to the magnitude squared of the sum of three algebraic expressions corresponding to the three physical basis functions. This sum is

$$I = e^{-jk_0\frac{h}{2}\sin\phi_W}\sum_{n=1}^{3} A_n \frac{\sin\left[\frac{w}{2}(k_0\cos\phi - g_n)\right]}{\frac{w}{2}(k_0\cos\phi - g_n)} \times \left\{c_{xn}\sin\phi + \frac{j\omega\varepsilon_0(\varepsilon_r-1)}{f_n^2 - k_0^2\sin^2\phi}\left[c_{xn}\zeta_x\sin\phi - c_{yn}\zeta_y\cos\phi\right]\right\} \quad (95)$$

where $\zeta_x = e^{jk_0h\sin\phi}\left[jk_0\sin\phi\sin(f_nh) - f_n\cos(f_nh)\right] + f_n$

$$\zeta_y = e^{jk_0 h \sin\phi} [jk_0 \sin\phi \sin(f_n h) + f_n \cos(f_n h)] - jk_0 \sin\phi \tag{96}$$

Note the $\sin(x)/x$ envelope which is dependent on the strip width w An advantageous feature is that we can isolate the contribution of each of the three physical basis functions to the overall σ_{2D}. For instance, we expect the scattered fields due to the "forced" wave to be maximal in the specular direction.

V. *Results and Conclusions*

The equations developed in the Chapter IV were coded in standard FORTRAN and compiled and executed on a microVAX 3+ computer using the VMS version 5.3 operating system. The program, called PBFSTRIP, reads geometry and material parameters from an input file, generates the impedance and voltage matrices, solves for the unknown current vector (using Irvin's matrix inversion routine (11)), and writes the surface wave parameters, solution errors, strip and dielectric currents, and bistatic scattering width to output files. A description and source-code listing of PBFSTRIP may be found in the supplement to this thesis.

In this chapter, we present some results from running PBFSTRIP and evaluate its performance. We investigate the convergence of the solution as the number and configuration of match points is varied. We compare the accuracy of the results and execution time to data provided by Dr. Kent of Mission Research Corporation, using a pulse-Galerkin moment method implementation.

We expect the physical basis functions to accurately represent the conduction and polarization currents near the middle of the scatterer, but not near the edges where the scatterer does not resemble an infinite structure. Additionally, the physical basis functions do not model the diffractions from the corners of the dielectric slab and the edges of the conducting strip.

We found that only the Z^x_{mn} impedance matrix needed to be included in PBFSTRIP and that Z^y_{mn} and Z^z_{mn} contributed nothing to the correct solution. We surmise this is because the most important boundary condition that must be met is that of vanishing tangential electric field on the conductor, $E^T_x(x, -\frac{h}{2}) = 0$, which only the Z^x_{mn} impedance matrix addresses directly.

5.1 The Run Matrix

We wish to observe the behavior of the results as the input parameters vary. The input parameters consist of relative permittivity ϵ_r, slab width w and thickness h, and angle of incidence θ, measured counterclockwise from the positive y-axis. We thus generate a run matrix by defining

Case	ϵ_r	w/λ_0	h/λ_0	θ (deg)	Comment
0	5	5	0.05	-30	Baseline
1	2	5	0.05	-30	Small ϵ_r
2	8.28	5	0.05	-30	Large ϵ_r
3	5	3	0.05	-30	Small w
4	5	10	0.05	-30	Large w
5	5	5	0.025	-30	Small h
6	5	5	0.10	-30	Large h
7	5	5	0.05	0	Normal Incidence
8	5	5	0.05	-60	Near Grazing Incidence
9	5	5	0.05	-85	Grazing Incidence

Table 1. Run Matrix

a baseline configuration and perturbing the input parameters individually about the baseline value The run matrix is shown in Table 5.1.

5.2 Convergence of the Solution for Various Match Point Configurations

Although PBFSTRIP is written to accept match points both within the dielectric and on the conductor, we find experimentally that only the match points on the conductor are significant This is probably due to the dominance of the strict boundary condition on the strip (vanishing $\vec{E}_x^T$) The question remains as to how many match points to take on the conductor, and how they should be distributed

We ran several cases at normal incidence, $\theta = 0°$, a geometry that will give us forward and reverse surface waves (FSW and RSW, respectively) of equal amplitude To achieve this, we find we must have a symmetric match point distribution with respect to the left and right edges of the strip. This is equivalent to weighting the FSW and RSW equally.

Using symmetric distributions, we wish to determine the effects of different numbers of match points, and how close to the edges we may place them. We repeated each case in the run matrix with 5, 9, 17, and 21 match points on the conductor to test for convergence of the solution. The results for the baseline Case 0 are presented in Table 5.2; the other cases show similar trends "Range" refers to the portion of the strip over which the match points are distributed and CN is

M	Range	Wave Amplitude			CN	Avg Rel Error
		Forced Wave	FSW	RSW		
5	0.3-0.7	1.067∠ − 22.4°	0.000646∠ − 59.6°	0.001341∠106.8°	46.3	0.000642
9	0.3-0.7	1.067∠ − 22.3°	0.000310∠ − 86.1°	0.001045∠ 95.1°	15.3	0.002667
17	0.2-0.8	1.067∠ − 22.4°	0.000309∠ − 88.4°	0.001163∠100.4°	19.6	0.005103
21	0.1-0.9	1.070∠ − 22.4°	0.000471∠ − 78.6°	0.001491∠116.1°	17.7	0.012775

Table 2. Baseline Case Results for Various Match Point Configurations

the condition number of the normalized 3×3 impedance matrix

Several conclusions may be drawn from Table 5.2. First, the forced wave amplitude is insensitive to match point configuration, but the FSW and RSW amplitudes fluctuate moderately. Second, the RSW amplitude is greater than the FSW amplitude, which is not surprising if we think of the incident wave "feeding" the RSW at the right edge of the slab more strongly than the FSW at the left edge. Third, the normalized impedance matrix is numerically stable (low condition number) for all match point configurations. Fourth, the average relative error (see Equation 94) increases with the number of match points, but does not become unacceptably large. The overall conclusion is that the physical basis function solution converges even for relatively few match points.

5.3 Accuracy of the Solution

Convergence of the solution is only desirable if it converges to the correct values. We use data provided by Dr. Kent from a pulse-Galerkin code as truth data, and look for agreement both in the currents and in the scattered far-fields. All cases defined in Table 5.1 were run for $M = 5, 9, 17$, and 21, and the currents and far-fields for the PBF and pulse-Galerkin solutions overlaid in a common format. We compare PBFSTRIP and pulse-Galerkin results for the extremes of $M = 5$ and $M = 21$, these results are shown in Figures 5 through 14. Each figure is organized as follows. The upper left graph shows the conduction current J_c along the conducting strip. The upper right and lower left graphs show the x-directed and y-directed polarization currents, J^x_{eq} and J^y_{eq} respectively, along the middle of the dielectric slab. The lower right graph shows the bistatic scattering width σ_{2D} where the bistatic angle ϕ is measured counterclockwise from the positive

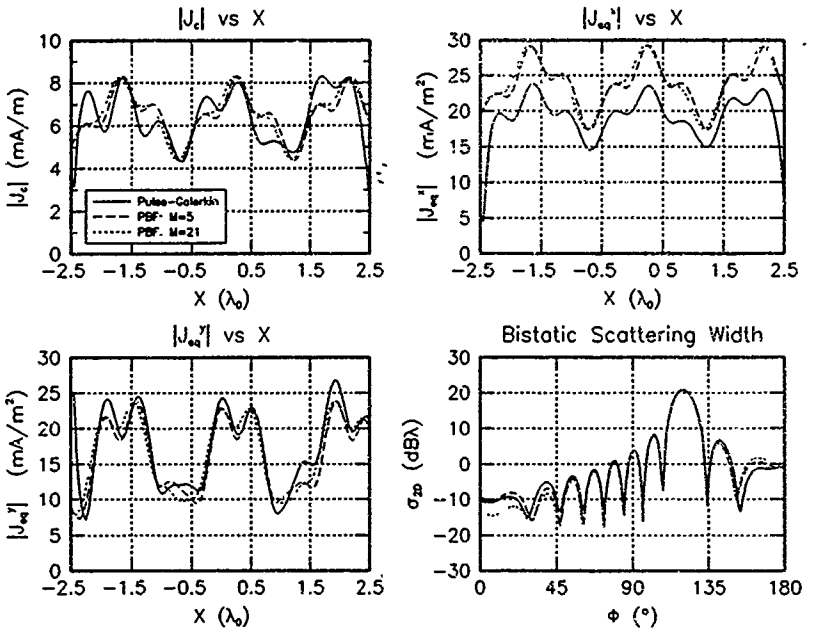

Figure 5. Case 0: $\varepsilon_r = 5.00$, $w = 5\ 0\lambda_0$, $h = 0\ 05\lambda_0$, $\theta = -30°$

x-axis.

In Figure 5 we see that the conduction current J_c predicted by the PBF and pulse-Galerkin solutions grossly agree, but there are differences on the order of 10% at five places on the strip. Additionally, the pulse-Galerkin J_c correctly vanishes at the strip edges while the PBF J_c does not. The pulse-Galerkin J^x_{eq} is an almost constant 10-20% below the PBF J^x_{eq}, but the locations of the "hills and valleys" agree well. Again, the pulse-Galerkin J^x_{eq} disappears at the edges while PBFSTRIP fails to predict this. The pulse-Galerkin J^y_{eq} and PBF J^y_{eq} agree very closely. The bistatic scattering widths predicted by the two solutions agree very closely in the number, locations, and widths of the main and side lobes. Both methods predict the main lobe in the specular direction

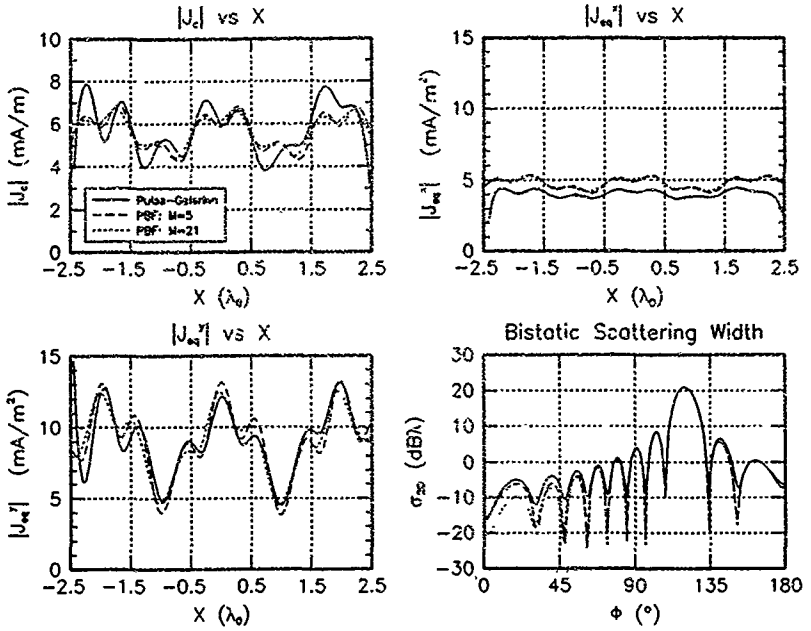

Figure 6. Case 1: $\epsilon_r = 2.00$, $w = 5\ 0\lambda_0$, $h = 0\ 05\lambda_0$, $\theta = -30°$

of $\phi = 120°$. The two solutions overlay almost exactly (within 1–2 dBλ) for ϕ between 30° and 150°, and are within 3 dB for the near-grazing bistatic angles $0° < \phi < 30°$ and $150° < \phi < 180°$ Notice that for Case 0, $M = 5$ agrees more closely with the pulse-Galerkin code than $M = 21$ in predicting the far-fields.

Case 1 is illustrated in Figure 6. Permittivity ϵ_r is small, and the polarization currents are correspondingly lower than in Case 0. The strip conduction current J_c predicted by the PBF and pulse-Galerkin solutions show the same rough equivalence as seen in Case 0 The scattering widths predicted by the two methods overlay almost exactly, although the far-field PBFSTRIP nulls are deeper than the pulse-Galerkin nulls Otherwise, the largest disagreement is about 5 dBλ

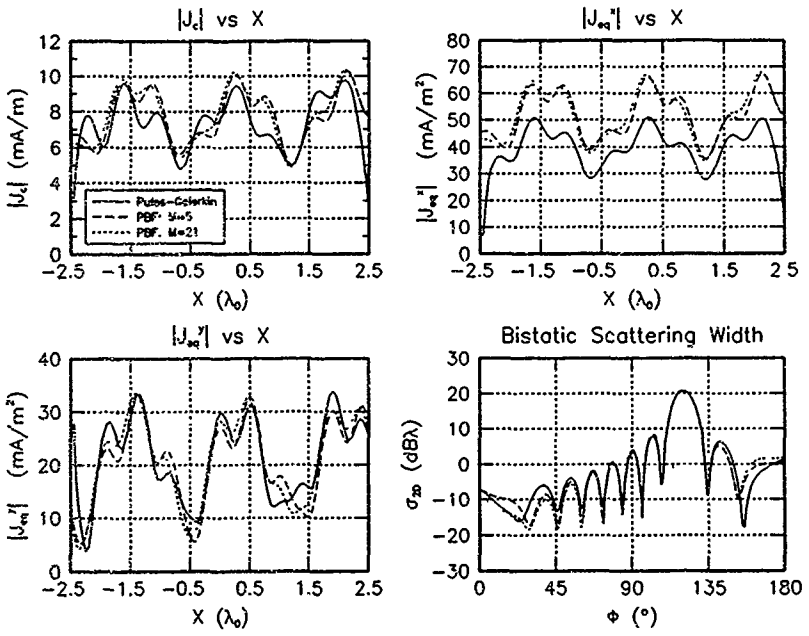

Figure 7 Case 2: $\epsilon_r = 8.28$, $w = 5.0\lambda_0$, $h = 0\ 05\lambda_0$, $\theta = -30°$

at $\phi = 20°$

Case 2 is illustrated in Figure 7. Permittivity ϵ_r is large, and the polarization currents are much higher than in Case 0. The strip and polarization currents predicted by the two methods show the same characteristics as noted for Cases 0 and 1. The far-field disagreement is about 4 dBλ for $0° < \phi < 45°$ and $150° < \phi < 180°$ and the outermost nulls are displaced about 4°: otherwise the far-fields overlay almost exactly.

Case 3 is depicted in Figure 8. Strip width w is small, and the far-field lobes are correspondingly wider than in Case 0. The PBFSTRIP and pulse-Galerkin conduction and polarization currents show qualitatively poorer agreement than for the previous cases, although $M = 21$ agrees

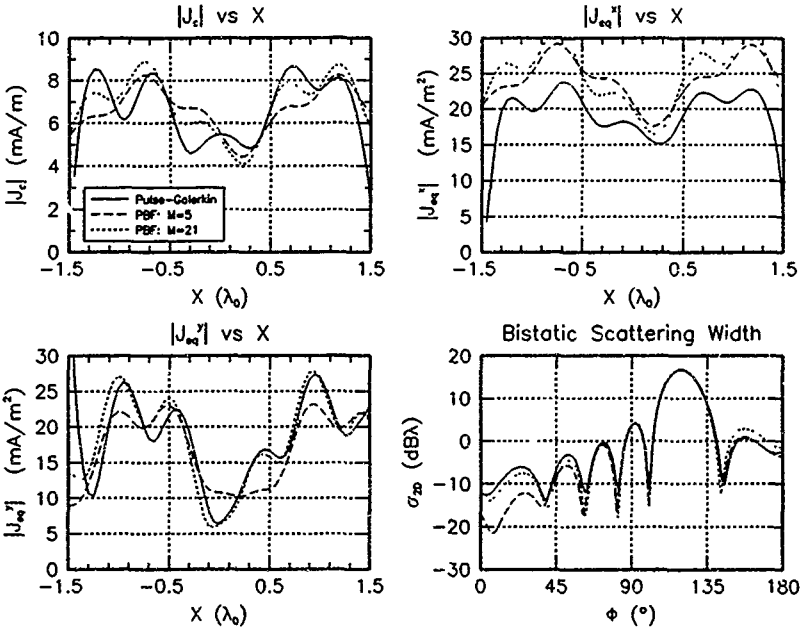

Figure 8. Case 3: $\epsilon_r = 5.00$, $w = 3.0\lambda_0$, $h = 0.05\lambda_0$, $\theta = -30°$

more closely than $M = 5$. The far-fields agree very well, for $M = 21$ the maximum disagreement is less than 2 dBλ over the entire $0° < \phi < 180°$ bistatic range. When $M = 5$, however, the far-fields disagree by as much as 10 dBλ for $0° < \phi < 35°$.

Case 4 is shown in Figure 9. Strip width w is large and the far-field lobes are correspondingly narrower than in Case 0. The PBFSTRIP and pulse-Galerkin currents are roughly the same. The far-fields overlay almost exactly except near grazing ($0° < \phi < 45°$, $155° < \phi < 180°$). However, there may be a problem with the pulse-Galerkin solution in this case, as evidenced by the very deep null at $\phi = 8°$; all other cases have a nearly constant scattering width when $0° < \phi < 30°$. This null is suspect because, due to the large width of the slab, the pulse-Galerkin cell size had to

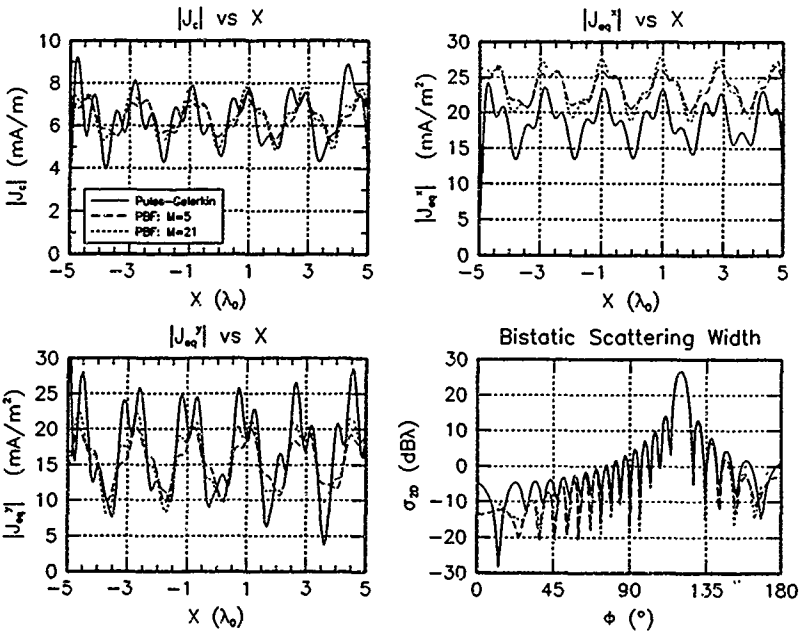

Figure 9 Case 4: $\epsilon_r = 5.00$, $w = 10.0\lambda_0$, $h = 0.05\lambda_0$, $\theta = -30°$

be raised above the convergence threshold of $\lambda_d/10$ to $\lambda_d/9$.

Case 5 is illustrated in Figure 10. The slab is half as thick as in Case 0. As before, the PBFSTRIP and pulse-Galerkin currents are roughly equivalent, although the PBFSTRIP J^x_{eq} is nearly twice as large as the pulse-Galerkin J^x_{eq}. The far-fields overlay almost exactly except for $0° < \phi < 50°$, where the PBFSTRIP scattering width is as much as 5 dBλ lower than the pulse-Galerkin scattering width. Also, the PBFSTRIP nulls are 10–15 dBλ below the pulse-Galerkin nulls.

Case 6 is shown in Figure 11. The dielectric slab is twice as thick as in Case 0, although not thick enough to allow higher-order surface wave modes to cut on ($\frac{h}{\lambda_0} \leq \frac{1}{4\sqrt{\epsilon_r - 1}}$) For the pulse-

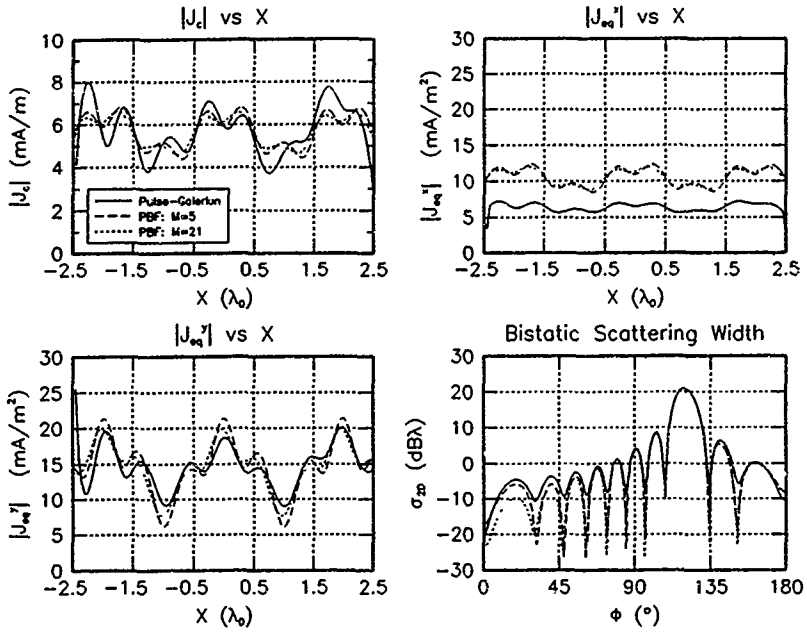

Figure 10. Case 5: $\varepsilon_r = 5.00$, $w = 5.0\lambda_0$, $h = 0.025\lambda_0$, $\theta = -30°$

Galerkin solution, we are forced into using a cell size of $\lambda_d/5$, so the pulse-Galerkin results are suspect Still, the currents predicted by the two methods agree fairly well, although the currents appear to be "shifted" spatially on the x-axis by about $0.25\lambda_0$ The far-fields agree fairly closely, except in the region $25° < \phi < 50°$ where the PBFSTRIP scattering width is 10 to 15 dB below the pulse-Galerkin prediction

Case 7 is depicted in Figure 12. The slab is illuminated at normal incidence ($\theta = 0°$), and the main lobe is in the backscatter ($\phi = 90°$) direction. Both PBFSTRIP and the pulse-Galerkin solution show the expected left-to-right symmetry in the currents. This geometry allows us to clearly see the effects of the three physical basis functions; the forced wave currents are exclusively

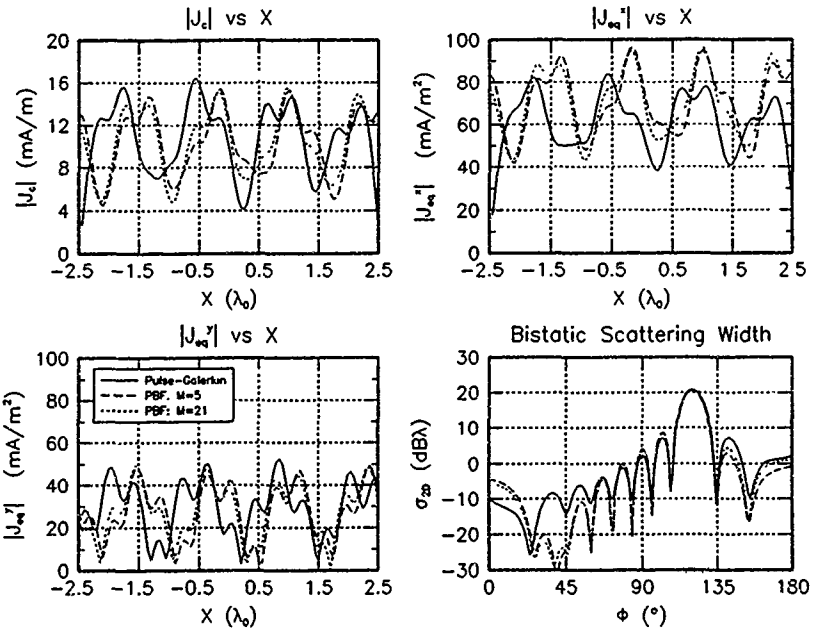

Figure 11. Case 6: $\varepsilon_r = 5.00$, $w = 5.0\lambda_0$, $h = 0.10\lambda_0$, $\theta = -30°$

x-directed and their phase is constant with respect to x, and the surface waves form a pure sinusoid pattern "riding" on the forced wave.

Another current component is evident in the pulse-Galerkin J_c, probably due to diffraction effects from the strip edges. The far-fields agree for $45° < \phi < 135°$ but differ significantly for bistatic angles closer to grazing. PBFSTRIP predicts two nulls in the angular region $0° < \phi < 45°$ while the pulse-Galerkin solution predicts -5 ± 2 dBλ for $0° < \phi < 40°$.

Case 8 is shown in Figure 13. The slab is illuminated at 60° from normal ($\theta = -60°$) The PBFSTRIP and pulse-Galerkin methods both predict a current distribution consisting of a low spatial frequency component with a "ripple" riding on it. This can be explained by a strong reverse

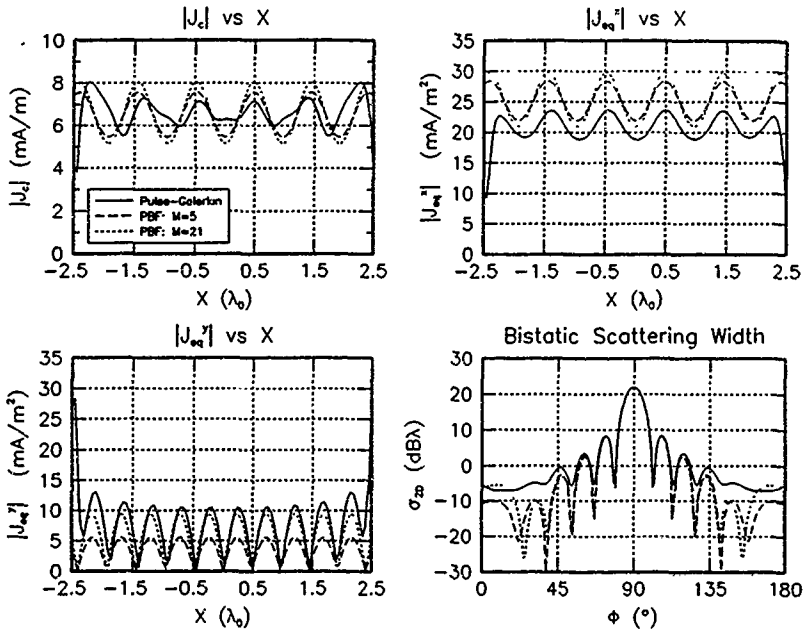

Figure 12. Case 7: $\epsilon_r = 5.00$, $w = 5.0\lambda_0$, $h = 0.05\lambda_0$, $\theta = 0°$

surface wave "beating against" the forced wave, and the low spatial frequency is determined by the difference in their x-directed phase constants. This corresponds to a "beat" wavelength of 5 $76\lambda_0$, corresponding fairly closely to the peak-to-valley distance of about $1.7\lambda_0$ shown in Figure 13 The far-fields agree fairly well except for $0° \lesssim \phi < 45°$ where the two solutions disagree by as much as 10 dBλ for $0° < \phi < 35°$.

Case 9 is illustrated in Figure 14, The slab is illuminated at very near grazing incidence, $\theta = -85°$. We see the same "beat" phenomenon as in Case 8, but now the "beat" wavelength is $23.3\lambda_0$, much longer than the strip width The PBFSTRIP and pulse-Galerkin currents are roughly equivalent except for a large, but uniform, disagreement in the J^y_{eq} The two scattering

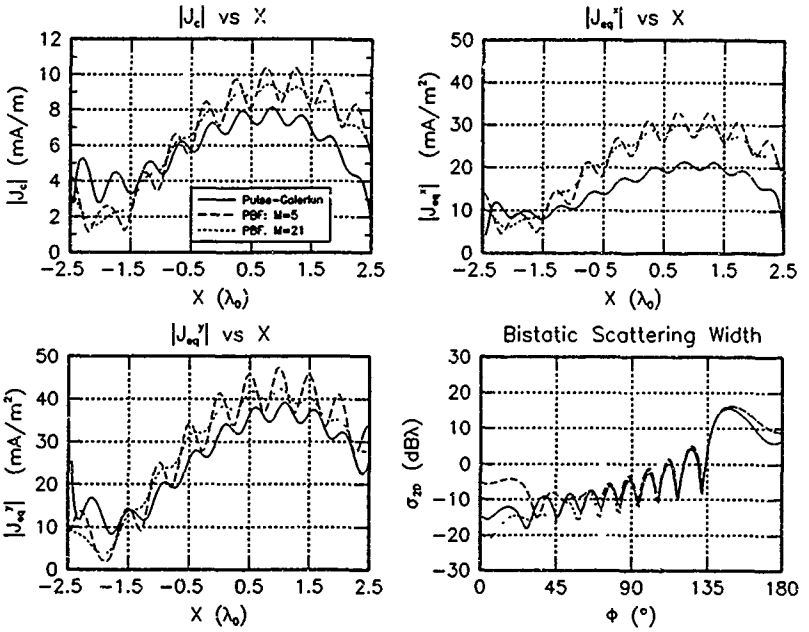

Figure 13. Case 8. $\epsilon_r = 5.00$, $w = 5.0\lambda_0$, $h = 0.05\lambda_0$, $\theta = -60°$

width predictions show the same trends and lobing patterns, but the PBFSTRIP scattering width prediction is 1 to 10 dB below the pulse-Galerkin prediction.

5.4 Execution Times

The real advantage of using a physical basis function solution is the reduced computer time and memory required when compared to subsectional solutions, such as the pulse-Galerkin technique considered here. The execution times for the ten test cases given in Table 5.1, as well as the dimension N of the pulse-Galerkin impedance matrix, are shown in Table 5.4. Both codes were run on a microVAX 3+.

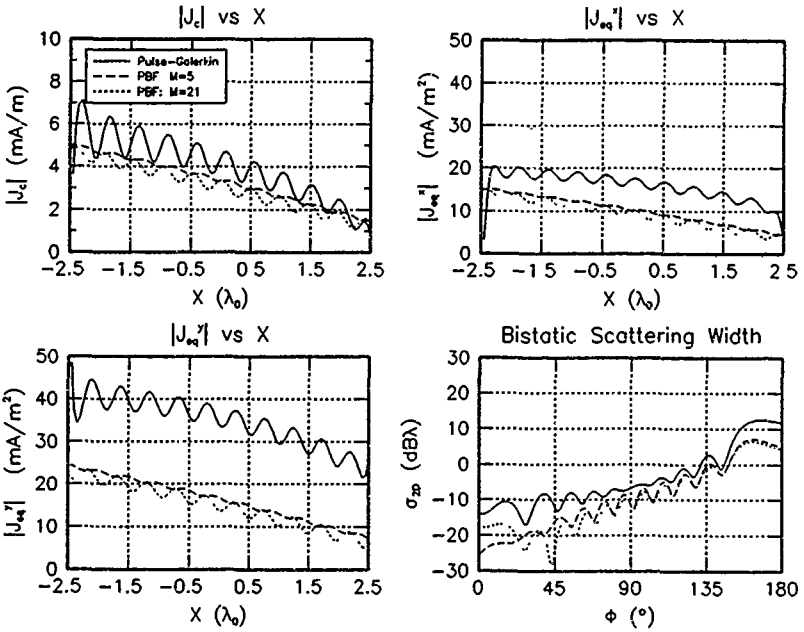

Figure 14 Case 9: $\varepsilon_r = 5.00$, $w = 5.0\lambda_0$, $h = 0\ 05\lambda_0$, $\theta = -85°$

The PBF solution executes about 10 times faster than the pulse-Galerkin solutions More importantly, the PBF solution does not depend strongly on the size of the scatterer, while the pulse-Galerkin solution execution time increases greatly with scatterer size.

The pulse-Galerkin solution uses most its execution time in solving the $N \times N$ impedance matrix by Gaussian elimination As reported by Woodworth (27), this time is proportional to N^3. The pulse size should be no larger than $\lambda_d/10$, where $\lambda_d = \lambda_0/\sqrt{\varepsilon_r}$ is the wavelength in the dielectric, so N is proportional to the size of the scatterer. Additionally, "heavy" dielectrics (large ε_r) require more pulses than light dielectrics, so N also increases with increasing ε_r.

The PBF solution expends most of its execution time in performing numerical integrations

Case	PBF CPU (sec)	Pulse-Galerkin N	Pulse-Galerkin CPU (sec)
0	23.5	300	286.4
1	24.1	300	285.3
2	23 1	300	281.4
3	14.7	180	83 8
4	25.0	540	1617.5
5	23.7	300	285 1
6	24.3	420	799.8
7	21.2	300	293.8
8	23.9	300	294.6
9	23.8	300	296.4

Table 3. Run Times: Physical Basis Function vs Pulse-Galerkin Solutions

to fill the $3 \times M$ impedance matrix. Negligible time is spent "normalizing" the impedance matrix (multiplying by its conjugate transpose) and solving the resultant 3×3 system of equations. The integration time increases with scatterer width, which is evident in Case 3 but not in Case 4, where the PBFSTRIP's integration algorithm increased the Gaussian quadrature node spacing rather than the number of nodes.

5 5 Components of the Far-Field

The use of physical basis functions allows us to gain some insight about how the different scattering mechanisms contribute to the total scattering width as a function of bistatic angle ϕ. Figure 15 shows the total scattering width and the contributions from the forced wave, FSW, and RSW for the baseline Case 0, $M = 5$. We see that the forced wave strongly dominates the scattering width for $35° < \phi < 150°$, being nearly 30 dB above the surface wave contributions at the main lobe. The surface wave contributions dominate the scattering width at near-grazing angles; the FSW dominates for $0° < \phi < 35°$ while the RSW dominates for $150° < \phi < 180°$. Another effect of the surface waves is to counter the deep forced wave nulls at 25°, 46°, 59°, and 154°.

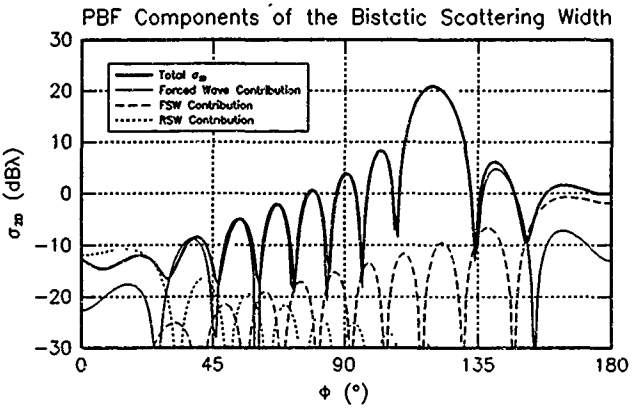

Figure 15. Baseline Case, 5 Match Points: $\varepsilon_r = 5.00$, $w = 5.0\lambda_0$, $h = 0.05\lambda_0$, $\theta = -30°$

5.6 Conclusions

The physical basis functions provide a reasonably complete and very efficient set in which to expand the currents and predict the far-fields for the dielectric-coated conducting strip

The PBF solution is relatively insensitive to the number of match points M so long as $M > 3$ Match points on the conductor work best, match points inside the dielectric slab do not contribute significantly to the solution A set of match points chosen symmetrically gives the best results

The PBF solution yields only roughly correct currents on the conductor and in the dielectric slab, but gives very accurate far-field predictions for incident and bistatic angles away from grazing At grazing bistatic angles, diffractions from the slab corners and strip edges become significant, and these contributions are not contained in the physical basis functions

The PBF solution runs an order of magnitude faster than a standard pulse-Galerkin moment method solution for scatterers of even modest dimensions ($5\lambda_0$ wide × $0.05\lambda_0$ thick). The PBF solution can be applied to large scatterers where the pulse-Galerkin solution simply cannot be used

If used with care, the speed of the PBF solution could allow us to find the far-fields for a range of different frequencies and apply Fourier analysis to predict a time-domain response of the scatterer

5.7 Recommendations

While the PBF solution and software developed in this thesis effort predicted the two-dimensional scattering width of a dielectric-coated conducting strip fairly well, it did not work well when the incident or bistatic angle was near grazing Unfortunately, agreement with the pulse-Galerkin currents was less than ideal In short, it was not perfect and can certainly be improved upon; additionally, its scope could be extended. Several areas where future research could explore follow

First, PBFSTRIP could be extended to include lossy and/or magnetic material. Lossy material would be relatively easy to incorporate; the only difficulty would be finding the surface wave phase constants from the transcendental equation (Equation 124) when ϵ_r is complex Müller's algorithm (16), as implemented by the IMSL subroutine ZANLY, could be used for this task The inclusion of a magnetic material ($\mu_d \neq \mu_0$) would be slightly more difficult to implement as the integral equations would then include an additional surface integration of the equivalent magnetic polarization current M^s_{eq}, as given by Equations 46, 51, and 55.

Second, the boundary conditions at the vertical edges of the dielectric slab and conducting strip are not satisfied; remember that the physical basis functions come from *infinite* structures that have no vertical boundaries The results clearly show that PBFSTRIP does not predict the necessary vanishing x- directed currents at the vertical boundaries. It would certainly be valid to devise a hybrid solution in which physical bases are used in the middle of the structure and a few rationally chosen subsectional basis functions are used at the edges. An example could be one-dimensional piecewise sinusoids on the strip and/or two-dimensional rooftop functions near the edges of the dielectric slab. Dr. Kent used this technique effectively for the simular problem of a

dielectric slab on an infinite ground plane illuminated by a TM^z plane wave.

Third, physical models of a dielectric-coated conducting strip could be fabricated and its bistatic scattering width could be measured in an anechoic chamber. Since a true two-dimensional model obviously is not physically realizable, a three-dimensional strip of length L could be made and its three- dimensional radar cross section σ_{3D} measured Then the two-dimensional scattering width σ_{2D} is given by (3.578)

$$\sigma_{2D} \simeq \frac{\lambda_0}{2L^2}\sigma_{3D} \qquad L \gg \lambda_0 \tag{97}$$

Appendix A. *Physical Basis Functions*

The physical basis functions are those wave components which exist on a dielectric-coated conducting strip of infinite width. In the limit as $w \to \infty$, the two-dimensional scattering geometry of Figure 1 degenerates into a one-dimensional dielectric-covered ground plane, as shown in Figure 16.

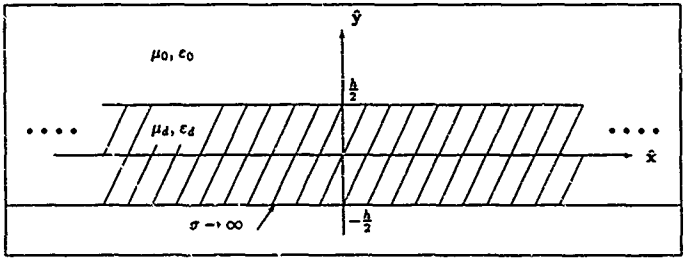

Figure 16 Dielectric-Covered Ground Plane

A.1 Forced Wave

Consider the geometry formed by a ground plane covered with a dielectric slab of height h. Let a TE^z uniform plane wave be incident on the dielectric, as shown in Figure 17, which sets up two uniform plane waves within the dielectric and a reflected uniform plane wave.

The electric fields in free space are composed of incident ($\vec{E}^i$) and reflected ($\vec{E}^r$) components. The fields in the dielectric are composed of "downward" ($\vec{E}^{d1}$) and "upward" ($\vec{E}^{d2}$) components. By Snell's Laws (3·191), $\theta = \theta_r$, $\theta_{d1} = \theta_{d2}$, and $k_d \sin\theta_d = k_o \sin\theta$ or $\sqrt{\epsilon_r}\sin\theta_d = \sin\theta$. We choose a reference point at $(0, \frac{h}{2})$ and arbitrarily force the fields to have zero phase at that point. We then write the electric fields explicitly as

$$\vec{E}^i(x,y) = E_o e^{-jk_o(x\sin\theta-(y-\frac{h}{2})\cos\theta)}(\hat{x}\cos\theta + \hat{y}\sin\theta) \tag{98}$$

$$\vec{E}^r(x,y) = Ae^{-jk_o(x\sin\theta+(y-\frac{h}{2})\cos\theta)}(\hat{x}\cos\theta - \hat{y}\sin\theta) \tag{99}$$

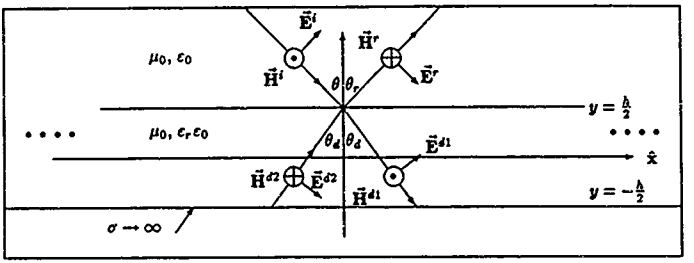

Figure 17. "Forced" Wave in Dielectric-Covered Ground Plane

$$\vec{E}^{d1}(x,y) = Be^{-jk_d(x\sin\theta_d-(y-\frac{h}{2})\cos\theta_d)}(\hat{x}\cos\theta_d+\hat{y}\sin\theta_d) \tag{100}$$

$$\vec{E}^{d2}(x,y) = Ce^{-jk_d(x\sin\theta_d+(y-\frac{h}{2})\cos\theta_d)}(\hat{x}\cos\theta_d-\hat{y}\sin\theta_d) \tag{101}$$

Without loss of generality, we let $E_o = 1$.

The magnetic fields are related to the electric fields through the impedance of the appropriate medium, and are given by

$$\vec{H}^i(x,y) = \hat{z}\frac{1}{\eta_o}e^{-jk_o(x\sin\theta-(y-\frac{h}{2})\cos\theta)} \tag{102}$$

$$\vec{H}^r(x,y) = -\hat{z}\frac{A}{\eta_o}e^{-jk_o(x\sin\theta+(y-\frac{h}{2})\cos\theta)} \tag{103}$$

$$\vec{H}^{d1}(x,y) = \hat{z}\frac{B}{\eta_d}e^{-jk_d(x\sin\theta_d-(y-\frac{h}{2})\cos\theta_d)} \tag{104}$$

$$\vec{H}^{d2}(x,y) = -\hat{z}\frac{C}{\eta_d}e^{-jk_d(x\sin\theta_d+(y-\frac{h}{2})\cos\theta_d)} \tag{105}$$

where $\eta_o = \sqrt{\mu_o/\varepsilon_o}$ and $\eta_d = \sqrt{\mu_d/\varepsilon_d} = \eta_o/\sqrt{\varepsilon_r}$. We are interested in the fields within the dielectric, which are given by

$$\begin{aligned}\vec{E}^d(x,y) &= \vec{E}^{d1}(x,y)+\vec{E}^{d2}(x,y)\\ \vec{H}^d(x,y) &= \vec{H}^{d1}(x,y)+\vec{H}^{d2}(x,y)\end{aligned} \tag{106}$$

We now apply the boundary conditions and solve for the unknown constants A, B, and C The first boundary condition requires that the total tangential electric field vanish along the dielec-

tric/conductor boundary. We arbitrarily choose the point $(0, -\frac{h}{2})$ and see that

$$E_x^{d1}\left(0,-\frac{h}{2}\right) + E_x^{d2}\left(0,-\frac{h}{2}\right) = Be^{-jk_d h\cos\theta_d}\cos\theta_d + Ce^{+jk_d h\cos\theta_d}\cos\theta_d = 0$$

or equivalently

$$B + Ce^{+j2k_d h\cos\theta_d} = 0 \tag{107}$$

The second boundary condition requires that the total tangential electric and magnetic fields be continuous across the free space/dielectric boundary. We arbitrarily choose the point $(0, \frac{h}{2})$ and see that

$$\begin{aligned} E_x^i\left(0,\frac{h}{2}\right) + E_x^r\left(0,\frac{h}{2}\right) &= E_x^{d1}\left(0,\frac{h}{2}\right) + E_x^{d2}\left(0,\frac{h}{2}\right) \\ H_x^i\left(0,\frac{h}{2}\right) + H_x^r\left(0,\frac{h}{2}\right) &= H_x^{d1}\left(0,\frac{h}{2}\right) + H_x^{d2}\left(0,\frac{h}{2}\right) \end{aligned}$$

Plugging into Equations 98–105, we can rewrite this as

$$\begin{aligned} \cos\theta + A\cos\theta &= B\cos\theta_d + C\cos\theta_d \\ \frac{1}{\eta_o} - \frac{A}{\eta_o} &= \frac{B}{\eta_d} - \frac{C}{\eta_d} \end{aligned}$$

or

$$A - B\frac{\cos\theta_d}{\cos\theta} - C\frac{\cos\theta_d}{\cos\theta} = -1 \tag{108}$$

$$A + B\frac{\eta_o}{\eta_d} - C\frac{\eta_o}{\eta_d} = 1 \tag{103}$$

We put Equations 107, 108, and 109 into matrix form

$$\begin{bmatrix} 0 & 1 & e^{+j2k_d h\cos\theta_d} \\ 1 & -\frac{\cos\theta_d}{\cos\theta} & -\frac{\cos\theta_d}{\cos\theta} \\ 1 & \frac{\eta_o}{\eta_d} & -\frac{\eta_o}{\eta_d} \end{bmatrix} \begin{bmatrix} A \\ B \\ C \end{bmatrix} = \begin{bmatrix} 0 \\ -1 \\ 1 \end{bmatrix} \tag{110}$$

From Equation 106, we only need to find B and C. Solving Equation 110, letting $\xi = k_d h \cos\theta_d$, and noting that $\eta_o/\eta_d = \sqrt{\epsilon_r}$, we find the following expressions for the B and C

$$B = \frac{\cos\theta\, e^{j\xi}}{\sqrt{\epsilon_r}\cos\theta\cos\xi + j\cos\theta_d \sin\xi} \tag{111}$$

$$C = \frac{-\cos\theta\, e^{-j\xi}}{\sqrt{\epsilon_r}\cos\theta\cos\xi + j\cos\theta_d \sin\xi} \tag{112}$$

We can now find expressions for the total electric field within the dielectric using Equations 100, 101, and 106. First, let us consider the x-component. Taking advantage of cancellations and remembering Snell's Law of Refraction, we find

$$\begin{aligned} E_x^d(x,y) &= \left[Be^{-jk_d(x\sin\theta_d-(y-\frac{h}{2})\cos\theta_d)} + Ce^{-jk_d(x\sin\theta_d+(y-\frac{h}{2})\cos\theta_d)}\right]\cos\theta_d \\ &= \left[e^{jk_d(y+\frac{h}{2})\cos\theta_d} - e^{-jk_d(y+\frac{h}{2})\cos\theta_d}\right]\frac{\cos\theta\,\cos\theta_d}{\sqrt{\epsilon_r}\cos\theta\cos\xi + j\cos\theta_d\sin\xi}e^{-jk_e x\sin\theta} \\ &= j\cos\theta_d\frac{2\cos\theta}{\sqrt{\epsilon_r}\cos\theta\cos\xi + j\cos\theta_d\sin\xi}\sin\left[k_d\cos\theta_d\left(y+\frac{h}{2}\right)\right]e^{-jk_e\sin\theta x} \end{aligned} \tag{113}$$

Similarly, we find the y-component of the electric field to be given by

$$\begin{aligned} E_y^d(x,y) &= \left[Be^{-jk_d(x\sin\theta_d-(y-\frac{h}{2})\cos\theta_d)} - Ce^{-jk_d(x\sin\theta_d+(y-\frac{h}{2})\cos\theta_d)}\right]\sin\theta_d \\ &= \frac{2\cos\theta\sin\theta_d}{\sqrt{\epsilon_r}\cos\theta\cos\xi + j\cos\theta_d\sin\xi}\cos\left[k_d\cos\theta_d\left(y+\frac{h}{2}\right)\right]e^{-jk_e\sin\theta x} \end{aligned} \tag{114}$$

The z-directed total magnetic field in the dielectric may be found using Equations 104, 105, and 106 and is given by

$$\begin{aligned} H_z^d(x,y) &= \frac{B}{\eta_d}e^{-jk_d(x\sin\theta_d-(y-\frac{h}{2})\cos\theta_d)} - \frac{C}{\eta_d}e^{-jk_d(x\sin\theta_d+(y-\frac{h}{2})\cos\theta_d)} \\ &= \frac{\sqrt{\epsilon_r}}{\eta_o}\frac{2\cos\theta}{\sqrt{\epsilon_r}\cos\theta\cos\xi + j\cos\theta_d\sin\xi}\cos\left[k_d\cos\theta_d\left(y+\frac{h}{2}\right)\right]e^{-jk_e\sin\theta x} \end{aligned} \tag{115}$$

A.2 Surface Waves

Consider the waveguide formed by a ground plane covered with a dielectric slab of height h, as shown in Figure 16. By applying the appropriate boundary conditions, we find that TM^z (odd) and TE^z (even) modes will propagate, but that the TM_0^z mode is dominant and has a cutoff frequency of zero. For thin dielectric slabs $\left(\frac{h}{\lambda_0} < \frac{1}{4\sqrt{\epsilon_r - 1}}\right)$, only the dominant TM_0^z mode will propagate unattenuated, and the electric fields within the dielectric are given by (8:163-164)

$$E_x(x,y) = \frac{A f^2}{j\omega\varepsilon_d} \sin\left[f\left(y+\frac{h}{2}\right)\right] e^{-j\beta z} \tag{116}$$

$$E_y(x,y) = -\frac{A f g}{\omega\varepsilon_d} \cos\left[f\left(y+\frac{h}{2}\right)\right] e^{-j\beta z} \tag{117}$$

$$E_z(x,y) = 0 \tag{118}$$

By Faraday's Law, $\vec{\mathbf{H}} = -\frac{1}{j\omega\mu_d}\nabla \times \vec{\mathbf{E}}$, the TM_0^z magnetic field is given by

$$H_x = H_y = 0 \tag{119}$$

$$H_z = -A f \cos\left[f\left(y+\frac{h}{2}\right)\right] e^{-j\beta z} \tag{120}$$

The propagation constants f and g may be found using (8:164)

$$(f\,h)\tan(f\,h) = \alpha h \epsilon_r \tag{121}$$

$$f^2 + g^2 = k_d^2 = \epsilon_r k_o^2 \tag{122}$$

$$-\alpha^2 + g^2 = k_o^2 = \omega^2 \mu_o \varepsilon_o \tag{123}$$

Equations 121–123 may be combined into

$$(f\,h)\tan(f\,h) = \epsilon_r h\sqrt{(\epsilon_r - 1)k_o^2 - f^2} \tag{124}$$

Equation 124 is a transcendental equation in the phase constant f whose solution(s) must be found numerically, although Richmond gives a graphical technique for real ϵ_r that is accurate to about

three figures (18). f is defined to be positive, but if f is negative the fields are unchanged except for a sign reversal of wave amplitude A. g is defined to be positive for a surface wave propagating in the $+x$-direction.

Furthermore, if $h < \frac{\lambda_0}{4\sqrt{\epsilon_r - 1}}$, then only one solution for f exists and lies within the range $0 \leq f \leq \frac{\pi}{2h}$. Once the phase constant f is found, phase constant g may be found using Equation 122 and the fields may be found using Equations 116–120.

The reverse surface wave has the same form as the forward surface wave. Phase constant g is negative, however, while phase constant f remains positive.

A.3 Phase Constants f and g

The surface waves and forced wave have the same form except for the amplitudes of the individual field components and phase constants in the x and y directions. We may compactly write expressions for the three types of waves as

$$E_{xn}(x,y) = A_n c_{xn} \sin\left[f_n\left(y+\frac{h}{2}\right)\right] e^{-jg_n x} \tag{125}$$

$$E_{yn}(x,y) = A_n c_{yn} \cos\left[f_n\left(y+\frac{h}{2}\right)\right] e^{-jg_n x} \tag{126}$$

$$H_{zn}(x,y) = A_n c_{zn} \cos\left[f_n\left(y+\frac{h}{2}\right)\right] e^{-jg_n x} \tag{127}$$

where $n = 1$ represents the forced wave, $n = 2$ represents the forward surface wave, and $n = 3$ represents the reverse surface wave. The unknown constant A_n is the amplitude of the n^{th} wave Phase constants f_n and g_n are given by Equation 113 for $n = 1$, and by Equations 122 and 124 for $n = 2$ and 3.

The known constants c_{xn}, c_{yn}, and c_{zn} define the relative amplitudes of the E_x, E_y, and H_z components of the n^{th} wave and are defined by Equations 116, 117, 120, 113, 114, and 115. Written in convenient matrix form, they are given by

$$\begin{bmatrix} c_{x1} & c_{x2} & c_{x3} \\ c_{y1} & c_{y2} & c_{y3} \\ c_{z1} & c_{z2} & c_{z3} \end{bmatrix} = \begin{bmatrix} j\cos\theta_d & \frac{f_2}{j\omega\varepsilon_d} & \frac{f_3}{j\omega\varepsilon_d} \\ \sin\theta_d & \frac{-g_2}{\omega\varepsilon_d} & \frac{-g_3}{\omega\varepsilon_d} \\ \sqrt{\varepsilon_r}/\eta_o & -1 & -1 \end{bmatrix} \tag{128}$$

where $\theta_d = \arcsin(\sin\theta/\sqrt{\varepsilon_r})$. Maxwell's equations (specifically, Ampere's and Gauss' Laws) allow us to relate the field amplitudes by

$$c_{xn} f_n + j c_{yn} g_n = j\omega\mu_0 c_{zn} = j k_0 \eta_0 c_{zn} \tag{129}$$

$$c_{yn} f_n + j c_{zn} g_n = 0 \tag{130}$$

Appendix B. *Calculation of Impedance Matrix Elements*

To fill the impedance matrix we must evaluate expressions involving the derivatives of surface and line integrals. We will find that the results are combinations of surface integrals over the dielectric slab cross-section, line integrals along the edges of the slab and along the conductor, and integrand evaluations at the corners of the slab and edges of the strip.

B.1 Impedance Matrix Element Z^x_{mn}

Z^x_{mn} is given by (see Equation 88)

$$\begin{aligned} Z^x_{mn} &= c_{xn}\sin(\xi_+)e^{-j\beta_n x_i} \\ &\quad -\frac{\epsilon_r-1}{4j}c_{xn}\left[k_o^2+\frac{\partial^2}{\partial x^2}\right]\iint_S \sin(\xi'_+)e^{-j\beta_n x'}H_0^{(2)}\left(k_o\sqrt{(x_i-x')^2+(y_j-y')^2}\right)dx'\,dy' \\ &\quad -\frac{\epsilon_r-1}{4j}c_{yn}\frac{\partial^2}{\partial x\partial y}\iint_S \cos(\xi'_+)e^{-j\beta_n x'}H_0^{(2)}\left(k_o\sqrt{(x_i-x')^2+(y_j-y')^2}\right)dx'\,dy' \\ &\quad +\frac{c_{zn}}{4\omega\epsilon_o}\left[k_o^2+\frac{\partial^2}{\partial x^2}\right]\int_C e^{-j\beta_n x'}H_0^{(2)}\left(k_o\sqrt{(x_i-x')^2+(y_j+\frac{h}{2})^2}\right)dx' \end{aligned} \tag{131}$$

where

$$\xi'_+ = f_n\left(\frac{h}{2}+y'\right) \tag{132}$$

$$\xi_+ = f_n\left(\frac{h}{2}+y_j\right) \tag{133}$$

$$\xi_- = f_n\left(\frac{h}{2}-y_j\right) \tag{134}$$

We introduce the change of variables $u = x' - x$ and $v = y' - y$ and re-write Equation 131 as

$$\begin{aligned} Z^x_{mn} &= c_{xn}\sin(\xi_+)e^{-j\beta_n x_i} \\ &\quad -\frac{(\epsilon_r-1)c_{xn}}{4j}\left[k_o^2+\frac{\partial^2}{\partial x^2}\right]\iint_{\hat{S}_m-\hat{S}_1}+\iint_{\hat{S}_1} \\ &\qquad \begin{bmatrix}\sin(\xi_+)\cos(f_n v)\\ +\cos(\xi_+)\sin(f_n v)\end{bmatrix} e^{-j\beta_n(x_i+u)}H_0^{(2)}\left(k_o\sqrt{u^2+v^2}\right)du\,dv \\ &\quad -\frac{(\epsilon_r-1)c_{yn}}{4j}\frac{\partial^2}{\partial x\partial y}\iint_{\hat{S}_m-\hat{S}_1}+\iint_{\hat{S}_1} \end{aligned}$$

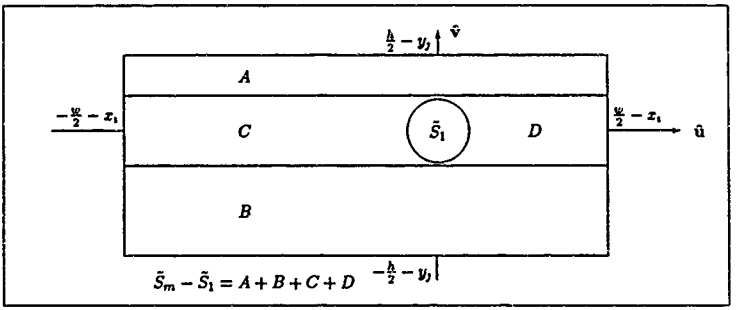

Figure 18. Integration Regions in uv-space

$$\left[\begin{array}{c}\cos(\xi_+)\cos(f_n v)\\ -\sin(\xi_+)\sin(f_n v)\end{array}\right] e^{-jg_n(x_i+u)} H_0^{(2)}\left(k_o\sqrt{u^2+v^2}\right)\,du\,dv$$

$$+\frac{c_{zn}}{4\omega\varepsilon_o}\left[k_o^2+\frac{\partial^2}{\partial z^2}\right]\int_{\tilde{C}_m} e^{-jg_n(x_i+u)} H_0^{(2)}\left(k_o\sqrt{u^2+(y_j+\frac{h}{2})^2}\right)\,du \qquad (135)$$

The regions of integration are depicted in Figure 18. The tilde on the regions of integration indicate integration over uv-space and the m subscript indicates dependence on the match point, (x_i, y_j) Region $\tilde{S}_1$ is a disk of radius R and is constant with respect to x_i and y_j.

$$\begin{aligned}
Z^z_{mn} \;=\;& c_{zn}\sin(\xi_+)\,e^{-jg_n x_i}\\
&-\frac{\varepsilon_r-1}{4j}\left[c_{zn}\left(k_o^2+\frac{\partial^2}{\partial x^2}\right)\sin(\xi_+)+c_{yn}\frac{\partial^2}{\partial x\partial y}\cos(\xi_+)\right]e^{-jg_n x_i}\times\\
&\iint_{\tilde{S}_m-\tilde{S}_1}\overbrace{\cos(f_n v)e^{-jg_n u}H_0^{(2)}\left(k_o\sqrt{u^2+v^2}\right)}^{F_1(u,v)}\,du\,dv\\
&-\frac{\varepsilon_r-1}{4j}\left[c_{zn}\left(k_o^2+\frac{\partial^2}{\partial x^2}\right)\cos(\xi_+)-c_{yn}\frac{\partial^2}{\partial x\partial y}\sin(\xi_+)\right]e^{-jg_n x_i}\times\\
&\iint_{\tilde{S}_m-\tilde{S}_1}\overbrace{\sin(f_n v)e^{-jg_n u}H_0^{(2)}\left(k_o\sqrt{u^2+v^2}\right)}^{F_2(u,v)}\,du\,dv\\
&-\frac{\varepsilon_r-1}{4j}\left[c_{zn}\left(k_o^2+\frac{\partial^2}{\partial x^2}\right)\sin(\xi_+)+c_{yn}\frac{\partial^2}{\partial x\partial y}\cos(\xi_+)\right]e^{-jg_n x_i}I^z_{sing}
\end{aligned}$$

$$+\frac{c_{zn}}{4\omega\epsilon_o}\left[k_o^2+\frac{\partial^2}{\partial x^2}\right]e^{-jg_n x_i}\int_{\tilde{C}_m} \overbrace{e^{-jg_n u}H_0^{(2)}\left(k_o\sqrt{u^2+(y_j+\frac{h}{2})^2}\right)}^{F_3(u,y)}\,du \qquad (136)$$

I^x_{sing} denotes the surface integral over the circular, or semicircular if $y_j = -\frac{h}{2}$, region $\tilde{S}_1$ that surrounds the singular origin in uv-space. I^x_{sing} is derived in detail in Appendix C.

When we evaluate the derivatives of the functions outside the integrals we find we can write

$$\begin{aligned}
Z^x_{imn} &= c_{zn}\sin(\xi_+)\,e^{-jg_n x_i} \\
&\quad -\frac{\epsilon_r-1}{4j}e^{-jg_n x_i}\sin(\xi_+)\left[c_{zn}\left(k_o^2-{g_n}^2\right)+jc_{yn}f_n g_n\right]I^x_{sing} \\
&\quad -\frac{\epsilon_r-1}{4j}e^{-jg_n x_i}\times \\
&\quad \left\{\begin{array}{l}
\left[c_{zn}(k_0^2-{g_n}^2)+jc_{yn}f_n g_n\right]\left[\sin(\xi_+)\iint F_1(u,v)\,du\,dv+\cos(\xi_+)\iint F_2(u,v)\,du\,dv\right] \\
-\left[c_{yn}f_n+j2c_{zn}g_n\right]\left[\sin(\xi_+)\frac{\partial}{\partial x}\iint F_1(u,v)\,du\,dv+\cos(\xi_+)\frac{\partial}{\partial x}\iint F_2(u,v)\,du\,dv\right] \\
-jc_{yn}g_n\left[\cos(\xi_+)\frac{\partial}{\partial y}\iint F_1(u,v)\,du\,dv-\sin(\xi_+)\frac{\partial}{\partial y}\iint F_2(u,v)\,du\,dv\right] \\
+c_{yn}\left[\cos(\xi_+)\frac{\partial^2}{\partial x\partial y}\iint F_1(u,v)\,du\,dv-\sin(\xi_+)\frac{\partial^2}{\partial x\partial y}\iint F_2(u,v)\,du\,dv\right] \\
+c_{zn}\left[\sin(\xi_+)\frac{\partial^2}{\partial x^2}\iint F_1(u,v)\,du\,dv+\cos(\xi_+)\frac{\partial^2}{\partial x^2}\iint F_2(u,v)\,du\,dv\right]
\end{array}\right\} \\
&\quad +\frac{c_{zn}}{4\omega\epsilon_0}e^{-jg_n x_i}\left[k_0^2-{g_n}^2-j2g_n\frac{\partial}{\partial x}+\frac{\partial^2}{\partial x^2}\right]\int_{\tilde{C}_m}F_3(u)\,du \qquad (137)
\end{aligned}$$

In Equation 137, functions F_1 and F_2 are integrated over region $\tilde{S}_m-\tilde{S}_1$. We evaluate the derivatives of the integrals using a simplified form of Leibnitz' Rule, applicable when the integrand is not a function of x (1:478)

$$\frac{\partial}{\partial x}\int_{f(x)}^{g(x)}F(\alpha)\,d\alpha = F[g(x)]\frac{\partial}{\partial x}g(x)-F[f(x)]\frac{\partial}{\partial x}f(x)$$

and find we can write

$$\frac{\partial}{\partial x}\iint_{\tilde{S}_m-\tilde{S}_1}F_1(u,v)\,du\,dv = e^{jg_n x_i}\left[e^{jg_n\frac{h}{2}}I_{mnc}-e^{-jg_n\frac{h}{2}}I_{mne}\right] \qquad (138)$$

$$\frac{\partial}{\partial z}\iint_{\tilde{S}_m-\tilde{S}_1}F_2(u,v)\,du\,dv = e^{jg_n x_i}\left[e^{jg_n\frac{h}{2}}I_{mnd}-e^{-jg_n\frac{h}{2}}I_{mnf}\right] \qquad (139)$$

$$\frac{\partial}{\partial x}\int_{\hat{C}_m} F_3(u,y)\,du = e^{jg_n x_i}\left[e^{jg_n\frac{w}{2}}H_0^{(2)}(k_0(++)) - e^{-jg_n\frac{w}{2}}H_0^{(2)}(k_0(-+))\right] \quad (140)$$

$$\frac{\partial}{\partial y}\int\int_{\hat{S}_m-\hat{S}_i} F_1(u,v)\,du\,dv = \cos(\xi_+)I_{mnk} - \cos(\xi_-)I_{mnl} \quad (141)$$

$$\frac{\partial}{\partial y}\int\int_{\hat{S}_m-\hat{S}_i} F_2(u,v)\,du\,dv = -\sin(\xi_+)I_{mnk} - \sin(\xi_-)I_{mnl} \quad (142)$$

$$\frac{\partial}{\partial y}\int_{\hat{C}_m} F_3(u,y)\,du = -k_0 I_{mnm} \quad (143)$$

$$\frac{\partial^2}{\partial x\partial y}\int\int_{\hat{S}_m-\hat{S}_i} F_1(u,v)\,du\,dv = e^{jg_n x_i}\left\{\begin{array}{l}\cos(\xi_+)\left[\begin{array}{l}e^{jg_n\frac{w}{2}}H_0^{(2)}(k_0(++))\\ -e^{-jg_n\frac{w}{2}}H_0^{(2)}(k_0(-+))\end{array}\right]\\ -\cos(\xi_-)\left[\begin{array}{l}e^{jg_n\frac{w}{2}}H_0^{(2)}(k_0(+-))\\ -e^{-jg_n\frac{w}{2}}H_0^{(2)}(k_0(--))\end{array}\right]\end{array}\right\} \quad (141)$$

$$\frac{\partial^2}{\partial x\partial y}\int\int_{\hat{S}_m-\hat{S}_i} F_2(u,v)\,du\,dv = -e^{jg_n x_i}\left\{\begin{array}{l}\sin(\xi_+)\left[\begin{array}{l}e^{jg_n\frac{w}{2}}H_0^{(2)}(k_0(++))\\ -e^{-jg_n\frac{w}{2}}H_0^{(2)}(k_0(-+))\end{array}\right]\\ +\sin(\xi_-)\left[\begin{array}{l}e^{jg_n\frac{w}{2}}H_0^{(2)}(k_0(+-))\\ -e^{-jg_n\frac{w}{2}}H_0^{(2)}(k_0(--))\end{array}\right]\end{array}\right\} \quad (145)$$

$$\frac{\partial^2}{\partial x\partial y}\int_{\hat{C}_m} F_3(u,y)\,du = -e^{jg_n x_i}k_0\left(\frac{h}{2}+y_j\right)\left[\begin{array}{l}e^{jg_n\frac{w}{2}}\frac{H_1^{(2)}(k_0(++))}{(++)}\\ -e^{-jg_n\frac{w}{2}}\frac{H_1^{(2)}(k_0(-+))}{(-+)}\end{array}\right] \quad (146)$$

$$\frac{\partial^2}{\partial x^2}\int\int_{\hat{S}_m-\hat{S}_i} F_1(u,v)\,du\,dv = e^{jg_n x_i}\left\{\begin{array}{l}e^{jg_n\frac{w}{2}}\left[jg_n I_{mnc} - k_0(\frac{w}{2}+x_i)I_{mng}\right]\\ -e^{-jg_n\frac{w}{2}}\left[jg_n I_{mne} + k_0(\frac{w}{2}-x_i)I_{mnh}\right]\end{array}\right\} \quad (147)$$

$$\frac{\partial^2}{\partial x^2}\int\int_{\hat{S}_m-\hat{S}_i} F_2(u,v)\,du\,dv = e^{jg_n x_i}\left\{\begin{array}{l}e^{jg_n\frac{w}{2}}\left[jg_n I_{mnd} - k_0(\frac{w}{2}+x_i)I_{mni}\right]\\ -e^{-jg_n\frac{w}{2}}\left[jg_n I_{mnf} + k_0(\frac{w}{2}-x_i)I_{mnj}\right]\end{array}\right\} \quad (148)$$

$$\frac{\partial^2}{\partial x^2}\int_{\hat{C}_m} F_3(u,y)\,du = e^{jg_n x_i}\left\{\begin{array}{l}e^{jg_n\frac{w}{2}}\left[\begin{array}{l}jg_n H_0^{(2)}(k_0(++))\\ -k_0(\frac{w}{2}+x_i)\frac{H_1^{(2)}(k_0(++))}{(++)}\end{array}\right]\\ -e^{-jg_n\frac{w}{2}}\left[\begin{array}{l}jg_n H_0^{(2)}(k_0(-+))\\ +k_0(\frac{w}{2}-x_i)\frac{H_1^{(2)}(k_0(-+))}{(-+)}\end{array}\right]\end{array}\right\} \quad (149)$$

$$\frac{\partial^2}{\partial y^2}\int\int_{\hat{S}_m-\hat{S}_i} F_1(u,v)\,du\,dv = -f_n\left[\sin(\xi_+)I_{mnk} + \sin(\xi_-)I_{mnl}\right] - k_0\left[\cos(\xi_+)I_{mnm} + \cos(\xi_-)I_{mnn}\right] \quad (150)$$

$$\frac{\partial^2}{\partial y^2}\iint_{\hat{S}_m-\hat{S}_1} F_2(u,v)\,du\,dv = -f_n\left[\cos(\xi_+)I_{mnk}-\cos(\xi_-)I_{mnl}\right] + k_0\left[\sin(\xi_+)I_{mnm}-\sin(\xi_-)I_{mnn}\right] \tag{151}$$

where

$$I_{mna} = \iint_{\hat{S}_m-\hat{S}_1} F_2(u,v)\,du\,dv \tag{152}$$

$$I_{mnb} = \iint_{\hat{S}_m-\hat{S}_1} F_1(u,v)\,du\,dv \tag{153}$$

$$I_{mnc} = \int_{-\frac{h}{2}-y_j}^{\frac{h}{2}-y_j} \cos(f_n v)\,H_0^{(2)}\left(k_0\sqrt{(\frac{w}{2}+x_i)^2+v^2}\right)\,dv \tag{154}$$

$$I_{mnd} = \int_{-\frac{h}{2}-y_j}^{\frac{h}{2}-y_j} \sin(f_n v)H_0^{(2)}\left(k_0\sqrt{(\frac{w}{2}+x_i)^2+v^2}\right)\,dv \tag{155}$$

$$I_{mne} = \int_{-\frac{h}{2}-y_j}^{\frac{h}{2}-y_j} \cos(f_n v)H_0^{(2)}\left(k_0\sqrt{(\frac{w}{2}-x_i)^2+v^2}\right)\,dv \tag{156}$$

$$I_{mnf} = \int_{-\frac{h}{2}-y_j}^{\frac{h}{2}-y_j} \sin(f_n v)H_0^{(2)}\left(k_0\sqrt{(\frac{w}{2}-x_i)^2+v^2}\right)\,dv \tag{157}$$

$$I_{mng} = \int_{-\frac{h}{2}-y_j}^{\frac{h}{2}-y_j} \cos(f_n v)\frac{H_1^{(2)}\left(k_0\sqrt{(\frac{w}{2}+x_i)^2+v^2}\right)}{\sqrt{(\frac{w}{2}+x_i)^2+v^2}}\,dv \tag{158}$$

$$I_{mnh} = \int_{-\frac{h}{2}-y_j}^{\frac{h}{2}-y_j} \cos(f_n v)\frac{H_1^{(2)}\left(k_0\sqrt{(\frac{w}{2}-x_i)^2+v^2}\right)}{\sqrt{(\frac{w}{2}-x_i)^2+v^2}}\,dv \tag{159}$$

$$I_{mni} = \int_{-\frac{h}{2}-y_j}^{\frac{h}{2}-y_j} \sin(f_n v)\frac{H_1^{(2)}\left(k_0\sqrt{(\frac{w}{2}+x_i)^2+v^2}\right)}{\sqrt{(\frac{w}{2}+x_i)^2+v^2}}\,dv \tag{160}$$

$$I_{mnj} = \int_{-\frac{h}{2}-y_j}^{\frac{h}{2}-y_j} \sin(f_n v)\frac{H_1^{(2)}\left(k_0\sqrt{(\frac{w}{2}-x_i)^2+v^2}\right)}{\sqrt{(\frac{w}{2}-x_i)^2+v^2}}\,dv \tag{161}$$

$$I_{mnk} = \int_{-\frac{w}{2}-x_i}^{\frac{w}{2}-x_i} e^{-jf_n u}H_0^{(2)}\left(k_0\sqrt{u^2+(\frac{h}{2}+y_j)^2}\right)\,du \tag{162}$$

$$I_{mnl} = \int_{-\frac{w}{2}-x_i}^{\frac{w}{2}-x_i} e^{-jf_n u}H_0^{(2)}\left(k_0\sqrt{u^2+(\frac{h}{2}-y_j)^2}\right)\,du \tag{163}$$

$$I_{mnm} = \int_{-\frac{w}{2}-x_i}^{\frac{w}{2}-x_i} e^{-jf_n u}\frac{\frac{h}{2}+y_j}{\sqrt{u^2+(\frac{h}{2}+y_j)^2}}H_1^{(2)}\left(k_0\sqrt{u^2+(\frac{h}{2}+y_j)^2}\right)\,du \tag{164}$$

$$I_{mnn} = \int_{-\frac{w}{2}-x_i}^{\frac{w}{2}-x_i} e^{-jf_n u}\frac{\frac{h}{2}-y_j}{\sqrt{u^2+(\frac{h}{2}-y_j)^2}}H_1^{(2)}\left(k_0\sqrt{u^2+(\frac{h}{2}-y_j)^2}\right)\,du \tag{165}$$

$$(++) = \sqrt{(\frac{w}{2}+x_i)^2+(\frac{h}{2}+y_j)^2} \tag{166}$$

$$(+-) = \sqrt{(\frac{w}{2}+x_i)^2+(\frac{h}{2}-y_j)^2} \tag{167}$$

$$(-+) = \sqrt{(\frac{w}{2}-x_i)^2+(\frac{h}{2}+y_j)^2} \tag{168}$$

$$(--) = \sqrt{(\frac{w}{2}-x_i)^2+(\frac{h}{2}-y_j)^2} \tag{169}$$

Surface integrals I_{mna} and I_{mnb} and line integrals I_{mnc} through I_{mnn} may be evaluated numerically *except* that when the match point lies on the conductor, line integral I_{mnk} must be integrated analytically in the interval $|u| < R$ and I_{mnm} must be evaluated in the limit as $y_j \to -\frac{h}{2}$

Employing the same methods as used to calculate $I^{x,y,z}_{sing}$ in Appendix C and requiring $R \leq \frac{3}{k_0}$, we may write

$$\begin{aligned}
I_{mnk}|_{y=-\frac{h}{2}} &= \int_{-\frac{w}{2}-x_i}^{-R} + \int_{R}^{\frac{w}{2}-x_i} e^{-j\beta_n u} H_0^{(2)}(k_0 u)\,du + 2\int_0^R \cos(g_n u) H_0^{(2)}(k_0 u)\,du \\
&\simeq \int_{-\frac{w}{2}-x_i}^{-R} + \int_{R}^{\frac{w}{2}-x_i} e^{-j\beta_n u} H_0^{(2)}(k_0 u)\,du \\
&\quad + \frac{2}{k_0}\int_0^{k_0 R} \sum_{i=0}^{N}\sum_{k=0}^{6} \frac{(-1)^i (g_n/k_0)^{2i}}{(2i)!\,3^{2k}} [\alpha_k - j\beta_k \ln u] u^{2(i+k)}\,du \\
&\simeq \int_{-\frac{w}{2}-x_i}^{-R} + \int_{R}^{\frac{w}{2}-x_i} e^{-j\beta_n u} H_0^{(2)}(k_0 u)\,du \\
&\quad + 2R\sum_{i=0}^{N} \frac{(-1)^i (g_n R)^{2i}}{(2i)!} \sum_{k=0}^{6} \frac{(k_0 R/3)^{2k}}{2i+2k+1} \times \\
&\quad \{\alpha_k - j\beta_k [\ln(k_0 R) - frac12i+2k+1]\}
\end{aligned} \tag{170}$$

Evaluating I_{mnm} when the match point lies on the conductor must be done in the limit as $y_j \to -\frac{h}{2}$ We find the only contribution comes from the neighborhood of the singular point and is given by

$$\lim_{y_j \to -\frac{h}{2}} I_{mnm} = -j\frac{2}{k_0} \tag{171}$$

When we plug Equations 138-151 into Equation 137, we find that Z^x_{mn} is given by

$$Z^x_{mn} = c_{xn} \sin(\xi_+) e^{-j\beta_n x_i}$$

$$
\begin{aligned}
&-\frac{\varepsilon_r-1}{4j}e^{-jg_n x_i}c_{xn}k_0^2\left[\cos(\xi_+)\,I_{mna}+\sin(\xi_+)\,I_{mnb}+I^x_{sing}\right]\\
&+\frac{\varepsilon_r-1}{4}e^{-jg_n x_i}c_{yn}g_n\left[I_{mnk}-\cos(f_n h)I_{mnl}\right]\\
&-\frac{\varepsilon_r-1}{4j}c_{yn}\left\{\begin{array}{l}\left[e^{jg_n\frac{w}{2}}H_0^{(2)}(k_0(++))-e^{-jg_n\frac{w}{2}}H_0^{(2)}(k_0(-+))\right]\\ -\cos(f_n h)\left[e^{jg_n\frac{w}{2}}H_0^{(2)}(k_0(+-))-e^{-jg_n\frac{w}{2}}H_0^{(2)}(k_0(--))\right]\end{array}\right\}\\
&+\frac{\varepsilon_r-1}{4j}c_{xn}k_0\left\{\begin{array}{l}\sin(\xi_+)\left[e^{jg_n\frac{w}{2}}(\frac{w}{2}+x_i)I_{mng}+e^{-jg_n\frac{w}{2}}(\frac{w}{2}-x_i)I_{mnh}\right]\\ +\cos(\xi_+)\left[e^{jg_n\frac{w}{2}}(\frac{w}{2}+x_i)I_{mni}+e^{-jg_n\frac{w}{2}}(\frac{w}{2}-x_i)I_{mnj}\right]\end{array}\right\}\\
&+\frac{c_{xn}}{4\omega\varepsilon_0}e^{-jg_n x_i}(k_0^2-g_n{}^2)I_{mnk}\\
&+\frac{c_{xn}g_n\eta_0}{4jk_0}\left[e^{jg_n\frac{w}{2}}H_0^{(2)}(k_0(++))-e^{-jg_n\frac{w}{2}}H_0^{(2)}(k_0(-+))\right]\\
&-\frac{c_{xn}\eta_0}{4}\left[e^{jg_n\frac{w}{2}}(\frac{w}{2}+x_i)\frac{H_1^{(2)}(k_0(++))}{(++)}+e^{-jg_n\frac{w}{2}}(\frac{w}{2}-x_i)\frac{H_1^{(2)}(k_0(-+))}{(-+)}\right]
\end{aligned}
\tag{172}
$$

B.2 Impedance Matrix Element Z^y_{mn}

Impedance matrix element Z^y_{mn} is derived from Equation 78 and, after implementing the same change of variables as in the previous section, may be written as

$$
\begin{aligned}
Z^y_{mn} \;=\;& c_{yn}\cos(\xi_+)e^{-jg_n x_i}\\
&-\frac{(\varepsilon_r-1)c_{xn}}{4j}\frac{\partial^2}{\partial x\partial y}\iint_{\hat{S}_m-\hat{S}_i}+\iint_{\hat{S}_i}\\
&\qquad\left[\begin{array}{l}\sin(\xi_+)\cos(f_n v)\\ +\cos(\xi_+)\sin(f_n v)\end{array}\right]e^{-jg_n(x_i+u)}H_0^{(2)}\left(k_o\sqrt{u^2+v^2}\right)\,du\,dv\\
&-\frac{(\varepsilon_r-1)c_{yn}}{4j}\left[k_o^2+\frac{\partial^2}{\partial y^2}\right]\iint_{\hat{S}_m-\hat{S}_i}+\iint_{\hat{S}_i}\\
&\qquad\left[\begin{array}{l}\cos(\xi_+)\cos(f_n v)\\ -\sin(\xi_+)\sin(f_n v)\end{array}\right]e^{-jg_n(x_i+u)}H_0^{(2)}\left(k_o\sqrt{u^2+v^2}\right)\,du\,dv\\
&+\frac{c_{xn}}{4\omega\varepsilon_o}\frac{\partial^2}{\partial x\partial y}\int_{\hat{C}_m}e^{-jg_n(x_i+u)}H_0^{(2)}\left(k_o\sqrt{u^2+(y_i+\frac{h}{2})^2}\right)\,du
\end{aligned}
\tag{173}
$$

Grouping terms and evaluating the partial derivatives outside the integrals yields

$$
\begin{aligned}
Z^y_{mn} \;=\;& c_{yn}\cos(\xi_+)\,e^{-jg_n x_i} \\
& -\frac{\epsilon_r-1}{4j}e^{-jg_n x_i}\left[c_{yn}\left(k_o^2-f_n^{\,2}\right)-jc_{xn}f_n g_n\right] I^y_{sing} \\
& -\frac{\epsilon_r-1}{4j}e^{-jg_n x_i}\times \\
& \left\{\begin{array}{l}
\left[c_{yn}(k_0^2-f_n^{\,2})-jc_{xn}f_n g_n\right]\left[\cos(\xi_+)\iint F_1(u,v)\,du\,dv-\sin(\xi_+)\iint F_2(u,v)\,du\,dv\right] \\
+c_{xn}f_n\left[\cos(\xi_+)\frac{\partial}{\partial x}\iint F_1(u,v)\,du\,dv-\sin(\xi_+)\frac{\partial}{\partial x}\iint F_2(u,v)\,du\,dv\right] \\
-\left[2c_{yn}f_n+jc_{xn}g_n\right]\left[\sin(\xi_+)\frac{\partial}{\partial y}\iint F_1(u,v)\,du\,dv+\cos(\xi_+)\frac{\partial}{\partial y}\iint F_2(u,v)\,du\,dv\right] \\
+c_{xn}\left[\sin(\xi_+)\frac{\partial^2}{\partial x\partial y}\iint F_1(u,v)\,du\,dv+\cos(\xi_+)\frac{\partial^2}{\partial x\partial y}\iint F_2(u,v)\,du\,dv\right] \\
+c_{yn}\left[\cos(\xi_+)\frac{\partial^2}{\partial y^2}\iint F_1(u,v)\,du\,dv-\sin(\xi_+)\frac{\partial^2}{\partial y^2}\iint F_2(u,v)\,du\,dv\right]
\end{array}\right\} \\
& +\frac{c_{zn}}{4\omega\varepsilon_0}e^{-jg_n x_i}\left[-jg_n\frac{\partial}{\partial y}+\frac{\partial^2}{\partial x\partial y}\right]\int_{\tilde{C}_m} F_3(u,y_j)\,du
\end{aligned}
\tag{174}
$$

Plugging in the expressions for the partial derivatives of the integrals, as developed in the previous section, we find

$$
\begin{aligned}
Z^y_{mn} \;=\;& c_{yn}\cos(\xi_+)\,e^{-jg_n x_i} \\
& -\frac{\epsilon_r-1}{4j}e^{-jg_n x_i}c_{yn}k_0^2\left[\cos(\xi_+)\,I_{mnb}-\sin(\xi_+)\,I_{mna}+I^y_{sing}\right] \\
& -\frac{\epsilon_r-1}{4j}c_{xn}f_n\left\{\begin{array}{l}
\cos(\xi_+)\left[e^{jg_n\frac{w}{2}}I_{mnc}-e^{-jg_n\frac{w}{2}}I_{mnc}\right] \\
-\sin(\xi_+)\left[e^{jg_n\frac{w}{2}}I_{mnd}-e^{-jg_n\frac{w}{2}}I_{mnf}\right]
\end{array}\right\} \\
& -\frac{\epsilon_r-1}{4j}e^{-jg_n x_i}\left[c_{yn}f_n+jc_{xn}g_n\right]\sin(f_n h)I_{mnl} \\
& +\frac{\epsilon_r-1}{4j}c_{xn}\sin(f_n h)\left[e^{jg_n\frac{w}{2}}H_0^{(2)}(k_0(+-))-e^{-jg_n\frac{w}{2}}H_0^{(2)}(k_0(--))\right] \\
& +\frac{(\epsilon_r-1)c_{yn}k_0-c_{xn}g_n\eta_0}{4j}e^{-jg_n x_i}I_{mnm} \\
& +\frac{\epsilon_r-1}{4j}e^{-jg_n x_i}c_{yn}k_0\cos(f_n h)I_{mnn} \\
& -\frac{c_{xn}\eta_0}{4}\left(\frac{h}{2}+y_j\right)\left[e^{jg_n\frac{w}{2}}\frac{H_1^{(2)}(k_o(++))}{(++)}-e^{-jg_n\frac{w}{2}}\frac{H_1^{(2)}(k_o(-+))}{(-+)}\right]
\end{aligned}
\tag{175}
$$

B.3 *Impedance Matrix Element* Z^z_{mn}

The impedance matrix elements associated with the $\hat{\mathbf{z}}$ integral equation may be derived from Equation 79 and are given by

$$
\begin{aligned}
Z^z_{mn} \;=\;& c_{zn}\cos(\xi_+)e^{-jg_n x_i} \\
&+\frac{\omega\varepsilon_0(\varepsilon_r-1)c_{xn}}{4}\frac{\partial}{\delta y}\iint_{\hat{S}_m-\hat{S}_1}+\iint_{\hat{S}_1} \\
&\qquad\left[\begin{array}{l}\sin(\xi_+)\cos(f_n v)\\ \quad+\cos(\xi_+)\sin(f_n v)\end{array}\right]e^{-jg_n(x_i+u)}H_0^{(2)}\left(k_0\sqrt{u^2+v^2}\right)\,du\,dv \\
&-\frac{\omega\varepsilon_0(\varepsilon_r-1)c_{yn}}{4}\frac{\partial}{\partial x}\iint_{\hat{S}_m-\hat{S}_1}+\iint_{\hat{S}_1} \\
&\qquad\left[\begin{array}{l}\cos(\xi_+)\cos(f_n v)\\ \quad-\sin(\xi_+)\sin(f_n v)\end{array}\right]e^{-jg_n(x_i+u)}H_0^{(2)}\left(k_0\sqrt{u^2+v^2}\right)\,du\,dv \\
&+\frac{c_{zn}}{4j}\frac{\partial}{\partial y}\int_{\hat{C}_m}e^{-jg_n(x_i+v)}H_0^{(2)}\left(k_0\sqrt{u^2+(\frac{h}{2}+y_j)^2}\right)\,du
\end{aligned}
\tag{176}
$$

Again, evaluating the derivatives outside the integrals, we find

$$
\begin{aligned}
Z^z_{mn} \;=\;& c_{zn}\cos(\xi_+)e^{-jg_n x_i} \\
&+\frac{k_0(\varepsilon_r-1)}{4\eta_0}e^{-jg_n x_i}\left\{c_{zn}f_n+jc_{yn}g_n\right\}I^z_{sing} \\
&+\frac{k_0(\varepsilon_r-1)}{4\eta_0}e^{-jg_n x_i}\times \\
&\left\{\begin{array}{l}\left[c_{zn}f_n+jc_{yn}g_n\right]\left[\cos(\xi_+)\iint F_1(u,v)\,du\,dv-\sin(\xi_+)\iint F_2(u,v)\,du\,dv\right]\\ -c_{yn}\left[\cos(\xi_+)\frac{\partial}{\partial x}\iint F_1(u,v)\,du\,dv-\sin(\xi_+)\frac{\partial}{\partial x}\iint F_2(u,v)\,du\,dv\right]\\ +c_{zn}\left[\sin(\xi_+)\frac{\partial}{\partial y}\iint F_1(u,v)\,du\,dv+\cos(\xi_+)\frac{\partial}{\partial y}\iint F_2(u,v)\,du\,dv\right]\end{array}\right\} \\
&+\frac{c_{zn}}{4j}e^{-jg_n x_i}\frac{\partial}{\partial y}\int_{\hat{C}_m}F_3(u,y_j)\,du
\end{aligned}
\tag{177}
$$

Plugging in expressions for the derivatives of the integrals, and implementing Equation 129, yields

$$
Z^z_{mn} \;=\; c_{zn}\cos(\xi_+)e^{-jg_n x_i}
$$

$$
\begin{aligned}
&-\frac{\varepsilon_r-1}{4j}c_{zn}k_0^2e^{-js_{xn}x_i}\left[\cos(\xi_+)I_{mns}-\sin(\xi_+)I_{mne}+I^i_{sing}\right]\\
&-\frac{k_0(\varepsilon_r-1)c_{yn}}{4\eta_0}\left\{\begin{array}{l}\cos(\xi_+)\left[e^{js_{xn}\frac{w}{2}}I_{mnc}-e^{-js_{xn}\frac{w}{2}}I_{mnc}\right]\\ \quad-\sin(\xi_+)\left[e^{js_{xn}\frac{w}{2}}I_{mnd}-e^{-js_{xn}\frac{w}{2}}I_{mnf}\right]\end{array}\right\}\\
&-\frac{k_0(\varepsilon_r-1)c_{zn}}{4\eta_0}e^{-js_{xn}x_i}\sin(f_nh)I_{mnl}\\
&-\frac{k_0c_{zn}}{4j}e^{-js_{xn}x_i}I_{mnm}
\end{aligned}
\tag{178}
$$

Appendix C. *Integration in the Neighborhood of the Singularity*

To fill the impedance matrix, as defined by Equations 172, 175, and 178 in Appendix B we must evaluate integrals whose integrands have singularities at the origin. Specifically, these integrals are

$$I^x_{sing}(y) = \iint_{\tilde{S}_1} \sin\left[f_n\left(v+y+\frac{h}{2}\right)\right] e^{-jf_n u} H_0^{(2)}\left(k_0\sqrt{u^2+v^2}\right)\,du\,dv \tag{179}$$

$$I^y_{sing}(y) = \iint_{\tilde{S}_1} \cos\left[f_n\left(v+y+\frac{h}{2}\right)\right] e^{-jf_n u} H_0^{(2)}\left(k_0\sqrt{u^2+v^2}\right)\,du\,dv \tag{180}$$

$$I^z_{sing}(y) = I^y_{sing}(y) \tag{181}$$

Region $\tilde{S}_1$ is a circle of radius R if the match point lies within the dielectric, or a semicircle of radius R if the match point lies on the conductor. Region $\tilde{S}_1$ is illustrated by Figure 19. We are

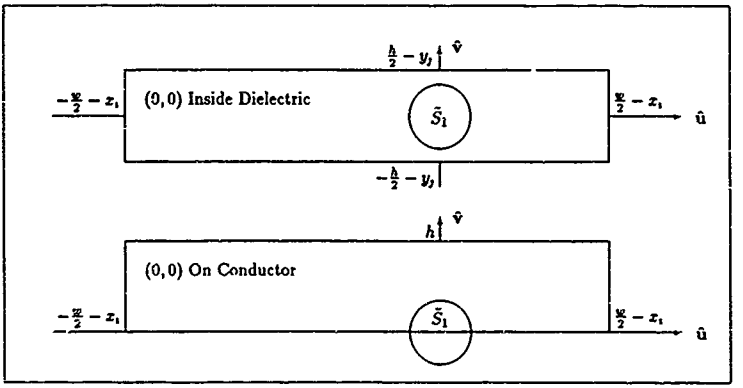

Figure 19. Region of Integration About the Singularity

also interested in evaluating partial derivatives of $I^{x,y,z}_{sing}$; these are given simply by

$$\frac{\partial}{\partial x} I^{x,y,z}_{sing} = 0 \tag{182}$$

$$\frac{\partial}{\partial y} I^{x}_{sing} = f_n I^{y,z}_{sing} \tag{183}$$

$$\frac{\partial}{\partial y} I^{x,z}_{sing} = -f_n I^{z}_{sing} \tag{184}$$

We consider separately the cases in which the match point lies inside the dielectric or on the conductor.

C.1 *Match Point Inside the Dielectric*

When the match point lies inside the dielectric ($y \neq -\frac{h}{2}$), region $\tilde{S}_1$ is a circle of radius R. Using Euler's Identity to turn the trigonometric terms into exponentials and switching to polar coordinates ($u = \rho\cos\theta, v = \rho\sin\theta$) allows us to write

$$I^{z}_{sing} = \frac{1}{2j} e^{jf_n(y+\frac{h}{2})} \overbrace{\int_0^{2\pi}\int_0^R e^{j\rho(f_n\sin\theta - g_n\cos\theta)} H_0^{(2)}(k_0\rho)\,\rho\,d\rho\,d\theta}^{I_1}$$
$$- \frac{1}{2j} e^{-jf_n(y+\frac{h}{2})} \overbrace{\int_0^{2\pi}\int_0^R e^{-j\rho(f_n\sin\theta + g_n\cos\theta)} H_0^{(2)}(k_0\rho)\,\rho\,d\rho\,d\theta}^{I_2} \tag{185}$$

$$I^{x,z}_{sing} = \frac{1}{2} e^{jf_n(y+\frac{h}{2})} I^{z}_1 + \frac{1}{2} e^{-jf_n(y+\frac{h}{2})} I^{z}_2 \tag{186}$$

These integrals have no dependence on the match point $(x,y)_m$ and thus need only be evaluated once, with the results applied to all impedance matrix elements whose match point lie in the interior of the dielectric. We reformulate the exponential using the identities

$$A\cos\phi + B\sin\phi = \sqrt{A^2+B^2}\,\cos\left[\phi - \arctan\left(\frac{B}{A}\right)\right] \tag{187}$$

$$\arctan\left(\frac{A}{B}\right) + \arctan\left(\frac{A}{-B}\right) = \mathrm{sgn}(A)\pi \tag{188}$$

$$\arctan\left(\frac{A}{B}\right) + \arctan\left(\frac{-A}{B}\right) = 0 \tag{189}$$

$$f_n{}^2 + g_n{}^2 = \epsilon_r k_0^2 \tag{190}$$

and write

$$I_1 = \int_0^R \rho H_0^{(2)}(k_0\rho) \int_0^{2\pi} e^{j\rho\sqrt{\epsilon_r}k_0\cos\left[\phi+\arctan\left(\frac{f_m}{f_n}\right)-\pi\right]}\, d\theta\, d\rho \tag{191}$$

$$I_2 = \int_0^R \rho H_0^{(2)}(k_0\rho) \int_0^{2\pi} e^{j\rho\sqrt{\epsilon_r}k_0\cos\left[\phi-\arctan\left(\frac{f_m}{f_n}\right)-\pi\right]}\, d\theta\, d\rho \tag{192}$$

Here we take the range of the arctan function to be $(-\pi, \pi]$ and must be careful to preserve the "sense" of the fraction $\frac{f_m}{f_n}$ (i e , $\arctan\left(\frac{-1}{2}\right) \neq \arctan\left(\frac{1}{-2}\right)$). Since the integration in θ covers a full period, the phase terms in the cosine functions don't matter, and integration in θ yields a zero-order Bessel function (17:360) and, rather fortuitously, $I_1 = I_2$. We may now write the one-dimensional integral in ρ as

$$I_1 = I_2 = 2\pi \int_0^R J_0(\sqrt{\epsilon_r}k_0\rho)\, H_0^{(2)}(k_0\rho)\, \rho\, d\rho \tag{193}$$

We scale the integration so that it is with respect to the argument of the Hankel function ($\tau = k_0\rho$), and write

$$I_1 = I_2 = \frac{2\pi}{k_0^2} \int_0^{k_0R} J_0(\sqrt{\epsilon_r}\tau)\, H_0^{(2)}(\tau)\, \tau\, d\tau \tag{194}$$

Requiring $\sqrt{\epsilon_r}k_0R < 3$, or $\frac{R}{\lambda_0} < \frac{3}{2\pi\sqrt{\epsilon_r}}$, we may replace the Bessel and Hankel functions by their seven-term small-argument polynomial expansions (as given in Appendix D) Integrating term-by-term, we find

$$I_1 = I_2 \simeq \pi R^2 \sum_{i=0}^{6}\sum_{k=0}^{6} \frac{a_i\epsilon_r^i}{i+k+1}\left(\frac{k_0R}{3}\right)^{2(i+k)} \times \left[\alpha_k - j\beta_k\left(\ln(k_0R) - \frac{1}{2(i+k+1)}\right)\right] \tag{195}$$

Plugging this result into Equation 185 and 186 allows us to write the final result as

$$I^e_{sing} = \sin\left[f_n\left(y+\frac{h}{2}\right)\right] I_1 \tag{196}$$

$$I^{y,z}_{sing} = \cos\left[f_n\left(y+\frac{h}{2}\right)\right] I_1 \tag{197}$$

C.2 Match Point on the Conductor

If the match point $(x,y)_m$ lies on the conductor, then we define the region $\tilde{S}_1$ to be a semicircle of radius R centered at the singular point (u,v)=(0,0), extending into the dielectric In a manner identical to that used in the previous section, and noting that $y+\frac{h}{2}=0$, we may write I^x_{sing} and $I^{y,z}_{sing}$ as

$$I^x_{sing} = \overbrace{\frac{1}{2j}\int_0^{\pi}\int_0^{R} e^{jk(f_m\sin\theta-g_m\cos\theta)}H_0^{(2)}(k_0\rho)\,\rho\,d\rho\,d\theta}^{I_1} - \overbrace{\frac{1}{2j}\int_0^{\pi}\int_0^{R} e^{-jk(f_m\sin\theta+g_m\cos\theta)}H_0^{(2)}(k_0\rho)\,\rho\,d\rho\,d\theta}^{I_2} \quad (198)$$

$$I^{y,z}_{sing} = \frac{1}{2}I_1+\frac{1}{2}I_2 \quad (199)$$

Converting to polar coordinates, we recast I_1 and I_2 as

$$I_1 = \int_0^{R}\rho\,H_0^{(2)}(k_0\rho)\int_0^{\pi} e^{jk\rho\sqrt{\epsilon_r}k_0\cos\left[\phi+\arctan\left(\frac{f_m}{g_m}\right)-\pi\right]}\,d\phi\,d\rho \quad (200)$$

$$I_2 = \int_0^{R}\rho\,H_0^{(2)}(k_0\rho)\int_0^{\pi} e^{jk\rho\sqrt{\epsilon_r}k_0\cos\left[\phi-\arctan\left(\frac{f_m}{g_m}\right)-\pi\right]}\,d\phi\,d\rho \quad (201)$$

We shift the interval of integration on ϕ and scale the integration in ρ and write

$$I_1 = \frac{1}{k_0^2}\int_0^{k_0R}\tau\,H_0^{(2)}(\tau)\int_{\arctan\left(\frac{f_m}{g_m}\right)-\pi}^{\arctan\left(\frac{f_m}{g_m}\right)} e^{j\sqrt{\epsilon_r}\tau\cos\theta}\,d\theta\,d\tau \quad (202)$$

$$I_2 = \frac{1}{k_0^2}\int_0^{k_0R}\tau\,H_0^{(2)}(\tau)\int_{-\arctan\left(\frac{f_m}{g_m}\right)-\pi}^{-\arctan\left(\frac{f_m}{g_m}\right)} e^{j\sqrt{\epsilon_r}\tau\cos\theta}\,d\theta\,d\tau \quad (203)$$

Again requiring $\frac{R}{\lambda_0}<\frac{3}{2\pi\sqrt{\epsilon_r}}$, we may replace the exponential and Hankel functions by their small-argument polynomial expansions (see Appendix D) Integrating term-by-term, we find the final expressions for I_1 and I_2 to be

$$I_1 \simeq R^2\sum_{i=0}^{N}\sum_{k=0}^{6}\frac{(j\sqrt{\epsilon_r})^i}{i!\,3^{2k}}\,\frac{(k_0R)^{i+2k}}{i+2k+2}\times$$

$$\left\{\alpha_k - j\beta_k\left[\ln(k_0R) - \frac{1}{i+2k+2}\right]\right\}\int_{\arctan\left(\frac{L_x}{L_y}\right)-\pi}^{\arctan\left(\frac{L_x}{L_y}\right)} \cos^i\theta\, d\theta \qquad (204)$$

$$I_2 \simeq R^2\sum_{i=0}^{N}\sum_{k=0}^{6}\frac{(j\sqrt{\varepsilon_r})^i}{i!\,3^{2k}}\frac{(k_0R)^{i+2k}}{i+2k+2}\times$$

$$\left\{\alpha_k - j\beta_k\left[\ln(k_0R) - \frac{1}{i+2k+2}\right]\right\}\int_{-\arctan\left(\frac{L_x}{L_y}\right)-\pi}^{-\arctan\left(\frac{L_x}{L_y}\right)} \cos^i\theta\, d\theta \qquad (205)$$

The integral in θ is straightforward (12.132) but has differing forms for i even or odd. Plugging Equations 204 and 205 into Equations 198 and 199, we may write

$$I^x_{sing} = \frac{1}{2j}(I_1 - I_2) \qquad (206)$$

$$I^{y,z}_{sing} = \frac{1}{2}(I_1 + I_2) \qquad (207)$$

The exponential series in Equations 204 and 205 are taken out to the $N+1^{th}$ term. The alternating nature of these series allows us to bound the error associated with their truncation by the sum of the first two terms neglected (1·293-4). For instance, letting $N = 10$ limits the relative truncation error in Equation 204 to less than 10^{-8}.

Appendix D. *Some Useful Series Expansions*

To fill the impedance matrix, as defined by Equation 185 and 198 in Appendix C, we must analytically evaluate integrals that do not appear in integral tables (12). We evaluate these integrals by expanding the functions in the integrand by their appropriate small-argument finite series approximations, multiplying the series together, interchanging orders of integration and summation, and integrating term-by-term In this Appendix, we present the series expansions used to approximate the functions appearing in the integrands of Equations 172, 175, and 178 in Appendix B.

D 1 Bessel Functions of Order Zero and One

Abramowitz & Stegun (17 369-370) present the following small-argument polynomial approximations for zero- and first-order Bessel, Neumann, and Hankel functions The arguments are real and confined to the interval $(0, 3]$.

$$J_0(x) \simeq \sum_{i=0}^{6} a_i \left(\frac{x}{3}\right)^{2i} \tag{208}$$

$$Y_0(x) \simeq \left(\frac{2}{\pi}\right) \ln\left(\frac{x}{2}\right) J_0(x) + \sum_{i=0}^{6} b_i \left(\frac{x}{3}\right)^{2i} \tag{209}$$

$$\begin{aligned} H_0^{(2)}(x) &= J_0(x) - jY_0(x) \\ &\simeq \sum_{i=0}^{6} (\alpha_i - j\beta_i \ln x) \left(\frac{x}{3}\right)^{2i} \end{aligned} \tag{210}$$

$$J_0(Cx)H_0^{(2)}(x) \simeq \sum_{i=0}^{6}\sum_{k=0}^{6} a_i C^{2i} [\alpha_k - j\beta_k \ln(x)] \left(\frac{x}{3}\right)^{2(i+k)} \tag{211}$$

The constants a_i, b_i, α_i, and β_i are given in Table 4 The absolute errors associated with these approximations are less than 5×10^{-8}.

Similarly, the small-argument polynomial expansions for Bessel, Neumann, and Hankel functions of order one are

$$J_1(x) \simeq x \sum_{i=0}^{6} c_i \left(\frac{x}{3}\right)^{2i} \tag{212}$$

Table 4. Coefficients for Bessel and Neumann Function Expansions, Order Zero

i	a_i	b_i	α_i	β_i
0	1.0000000	0 36746691	1.0000000+j0.0738043	0 63661977
1	-2.2499997	0.60559366	-2.2499997-j1.5984537	-1.43239430
2	1.2656208	-0.74350384	1.2656208+j1.3019858	0 80571923
3	-0.3163866	0 25300117	0.3163866-j0.3926135	-0.20141797
4	0.0444479	-0.04261214	0.0444479+j0.0622257	0 02829641
5	-0.0039444	0.00427916	-0.0039444-j0.0060197	-0.00251108
6	0 0002100	-0.00024846	0.0002100+j0.0003411	0.00013369

Table 5. Coefficients for Bessel and Neumann Function Expansions, Order One

i	c_i	d_i
0	0.50000000	-0 6366198
1	-0.56249985	0.2212091
2	0.21093573	2.1682709
3	-0.03954289	-1.3164827
4	0.00443319	0 3123951
5	-0.00031761	-0 0400976
6	0.00001109	0.0027873

$$Y_1(x) \simeq \left(\frac{2}{\pi}\right)\ln\left(\frac{x}{2}\right)J_1(x)+\frac{1}{x}\sum_{i=0}^{6}d_i\left(\frac{x}{3}\right)^{2i} \tag{213}$$

$$\begin{aligned} H_1^{(2)}(x) &= J_1(x)-jY_1(x) \\ &\simeq \sum_{i=0}^{6}\left\{\left[1+j\frac{\ln 4}{\pi}\right]c_i x - j\frac{2c_i}{\pi}x\ln x - j\frac{d_i}{x}\right\}\left(\frac{x}{3}\right)^{2i} \end{aligned} \tag{214}$$

where the constants c_i and d_i are given in Table 5 The absolute errors associated with these approximations are less than $1\,1\times10^{-7}$.

D 2 Hankel Functions Multiplied by Exponentials

We need to evaluate integrals of Hankel functions multiplied by complex exponentials, a task most easily performed by small-argument polynomial approximations Hankel function polynomial approximations are given in the previous section, exponentials may be approximated by (12 22,34)

$$\begin{aligned} e^{jCx} &= \sum_{i=0}^{\infty}\frac{(jC)^i}{i!}x^i \\ &\simeq \sum_{i=0}^{N/2}(-1)^i\left[1+\frac{jCx}{2i+1}\right]\frac{(Cx)^{2i}}{(2i)!} \qquad |x|<\infty \end{aligned} \tag{215}$$

$$\cos(Cx) \simeq \sum_{i=0}^{N} \frac{(-1)^i C^{2i}}{(2i)!} x^{2i} \tag{216}$$

The exponential series is written in this form to highlight its alternating nature, which allows us to bound the error associated with truncating the infinite series by the magnitude of the first term neglected (1:293-4). Combining series, we can then write

$$e^{jCx} H_0^{(2)}(x) \simeq \sum_{i=0}^{N/2} \sum_{k=0}^{6} \frac{(-1)^i C^{2i}}{(2i)!\, 3^{2k}} \left[1 + \frac{jCx}{2i+1}\right] [\alpha_k - j\beta_k \ln x] x^{2(i+k)} \tag{217}$$

$$\cos(Cx) H_0^{(2)}(x) \simeq \sum_{i=0}^{N} \sum_{k=0}^{6} \frac{(-1)^i C^{2i}}{(2i)!3^{2k}} [\alpha_k - j\beta_k \ln x] x^{2(i+k)} \tag{218}$$

Appendix E. *Derivatives of the Two-Dimensional Green's Function*

The two-dimensional free-space Green's function is given by (3 902)

$$G(x,y;x',y') = \frac{1}{4j}H_0^{(2)}(k_0R) \tag{219}$$

$$R = \sqrt{(x-x')^2+(y-y')^2} \tag{220}$$

where $H_0^{(2)}$ is the Hankel function of the second kind of order 0. We wish to find expressions for $\frac{\partial G}{\partial x}$, $\frac{\partial G}{\partial y}$, $\frac{\partial^2 G}{\partial x^2}$, $\frac{\partial^2 G}{\partial y^2}$, and $\frac{\partial^2 G}{\partial x \partial y} = \frac{\partial^2 G}{\partial y \partial x}$. We start with $\frac{\partial G}{\partial x}$. Using the chain rule and a Hankel function recurrence relation (17 361), $H_0^{(2)'}(k_0R) = -H_1^{(2)}(k_0R)$, we find the first partial derivative with respect to x to be

$$\begin{aligned}\frac{\partial G}{\partial x} &= \frac{dG}{dR}\frac{\partial R}{\partial x} \\ &= \left\{\frac{k_0}{4j}H_0^{(2)'}(k_0R)\right\}\left\{\frac{x-x'}{R}\right\} \\ &= j\frac{k_0(x-x')}{4R}H_1^{(2)}(k_0R)\end{aligned} \tag{221}$$

where the prime on the Hankel function denotes differentiation with respect to argument. By symmetry,

$$\frac{\partial G}{\partial y} = j\frac{k_0(y-y')}{4R}H_1^{(2)}(k_0R) \tag{222}$$

The second derivative with respect to x is

$$\begin{aligned}\frac{\partial^2 G}{\partial x^2} &= \frac{\partial}{\partial x}\frac{\partial G}{\partial x} \\ &= \frac{\partial}{\partial x}\left\{j\frac{k_0(x-x')}{4R}H_1^{(2)}(k_0R)\right\}\end{aligned}$$

Using the product rule, chain rule, and another Hankel function recurrence relation (17:361),

$$H_0^{(2)}(k_0R) - \frac{2}{k_0R}H_1^{(2)}(k_0R) = -H_2^{(2)}(k_0R)$$

we find

$$\begin{aligned}
\frac{\partial^2 G}{\partial x^2} &= \frac{jk_0}{4}\left\{\frac{H_1^{(2)}(k_0R)}{R}\frac{d}{dx}(x-x') + (x-x')H_1^{(2)}(k_0R)\frac{\partial R}{\partial x}\frac{d}{dR}\left(\frac{1}{R}\right)\right. \\
&\qquad \left. + \frac{(x-x')}{R}\frac{\partial R}{\partial x}\frac{d}{dR}H_1^{(2)}(k_0R)\right\} \\
&= \frac{jk_0}{4}\left\{\frac{H_1^{(2)}(k_0R)}{R} - \frac{(x-x')^2}{R^3}H_1^{(2)}(k_0R) + \frac{k_0(x-x')^2}{R^2}H_1^{(2)'}(k_0R)\right\} \\
&= \frac{jk_0}{4}\left\{\frac{H_1^{(2)}(k_0R)}{R} - \frac{(x-x')^2}{R^3}H_1^{(2)}(k_0R)\right. \\
&\qquad \left. + \frac{k_0(x-x')^2}{R^2}\left[H_0^{(2)}(k_0R) - \frac{1}{k_0R}H_1^{(2)}(k_0R)\right]\right\} \\
&= \frac{-k_0^2}{4j}\left\{\frac{1}{k_0R}H_1^{(2)}(k_0R) - \frac{(x-x')^2}{R^2}H_2^{(2)}(k_0R)\right\} \qquad (223)
\end{aligned}$$

Of special interest is the term

$$\begin{aligned}
\left[k_0^2 + \frac{\partial^2}{\partial x^2}\right]G &= k_0^2 G + \frac{\partial^2 G}{\partial x^2} \\
&= \frac{k_0^2}{4j}H_0^{(2)}(k_0R) - \frac{k_0^2}{4j}\left\{\frac{1}{k_0R}H_1^{(2)}(k_0R) - \frac{(x-x')^2}{R^2}H_2^{(2)}(k_0R)\right\} \\
&= \frac{k_0^2}{4j}\left\{H_0^{(2)}(k_0R) - \frac{1}{k_0R}H_1^{(2)}(k_0R) + \frac{(x-x')^2}{R^2}H_2^{(2)}(k_0R)\right\} \\
&= \frac{k_0^2}{4j}\left\{-H_2^{(2)}(k_0R) + \frac{1}{k_0R}H_1^{(2)}(k_0R) + \frac{(x-x')^2}{R^2}H_2^{(2)}(k_0R)\right\} \\
&= \frac{k_0^2}{4j}\left\{\frac{1}{k_0R}H_1^{(2)}(k_0R) - \frac{(y-y')^2}{R^2}H_2^{(2)}(k_0R)\right\} \qquad (224)
\end{aligned}$$

By symmetry,

$$\frac{\partial^2 G}{\partial y^2} = \frac{jk_0^2}{4}\left\{\frac{1}{k_0R}H_1^{(2)}(k_0R) - \frac{(y-y')^2}{R^2}H_2^{(2)}(k_0R)\right\} \qquad (225)$$

$$\left[k_0^2 + \frac{\partial^2}{\partial y^2}\right]G = \frac{k_0^2}{4j}\left\{\frac{1}{k_0R}H_1^{(2)}(k_0R) - \frac{(x-x')^2}{R^2}H_2^{(2)}(k_0R)\right\} \qquad (226)$$

Examination of these equations shows that

$$\nabla^2 G + k_0^2 G = \frac{\partial^2 G}{\partial x^2} + \frac{\partial^2 G}{\partial y^2} + k_0^2 G = 0 \qquad (227)$$

Using the recurrence relation $H_1^{(2)'}(k_0R) - \frac{1}{k_0R}H_1^{(2)}(k_0R) = -H_2^{(2)}(k_0R)$ (17 361), we find $\frac{\partial^2 G}{\partial x \partial y}$ to be given by

$$\begin{aligned}
\frac{\partial^2 G}{\partial x \partial y} &= \frac{\partial}{\partial y}\frac{\partial G}{\partial x} \\
&= \frac{\partial}{\partial y}\left\{ j\frac{k_0(x-x')}{4R}H_1^{(2)}(k_0R)\right\} \\
&= \frac{jk_0(x-x')}{4}\frac{\partial R}{\partial y}\frac{d}{dR}\left\{\frac{H_1^{(2)}(k_0R)}{R}\right\} \\
&= \frac{jk_0(x-x')(y-y')}{4R}\frac{k_0}{R}\left\{H_1^{(2)'}(k_0R) - \frac{H_1^{(2)}(k_0R)}{k_0R}\right\} \\
&= \frac{k_0^2}{4j}\frac{(x-x')(y-y')}{R^2}H_2^{(2)}(k_0R) \qquad (228)
\end{aligned}$$

Bibliography

1 Arfken, George. *Mathematical Methods for Physicists* (Third Edition). San Diego, CA Academic Press, Inc., 1985.

2 Arvas, E. et.al "E-Field Solution of TM-Scattering from Multiple Perfectly Conducting and Lossy Dielectric Cylinders of Arbitrary Cross- Section," *IEE Proceedings, Part H - Microwaves, Antennas and Propagation, 135*:115-123 (April 1986).

3 Balanis, Constantine A. *Advanced Engineering Electromagnetics*. New York: John Wiley, 1989.

4. Barksdale, Maj Harry H., Assistant Professor of Electrical Engineering Personal interview Air Force Institute of Technology, Wright-Patterson AFB OH, July 1990.

5 Blue, J L "Integral Equations for Electromagnetic Scattering by Wide Scatterers," *The Bell System Technical Journal, 59*.1893-1908 (December 1980).

6 Burket, Capt Harold D. *Electromagnetic Scattering from a Dielectric-Covered Plate*. MS thesis, AFIT/GE/ENG/89D-2, School of Engineering, Air Force Institute of Technology (AU), Wright-Patterson AFB OH, December 1989.

7 Burnside, W. D et al "A Technique to Combine the Geometrical Theory of Diffraction and the Moment Method," *IEEE Transactions on Antennas and Propagation, AP-23* 551-558 (July 1975)

8 Harrington, Roger F. *Time-Harmonic Electromagnetic Fields*. New York: McGraw-Hill, 1961

9 Harrington, Roger F. *Field Computation by Moment Methods* New York Macmillan, 1968

10 Huddleston, Philip L et al "Combined Field Integral Equation Formulation for Scattering by Dielectrically Coated Conducting Bodies," *IEEE Transactions on Antennas and Propagation, AP-34*:510-520 (April 1986)

11. Irvin, Capt William L. *A Method of Moments Solution for the Electric Currents on an Aperture-Fed Stacked Patch Microstrip Antenna* MS thesis, AFIT/GE/ENG/90D-27, School of Engineering, Air Force Institute of Technology (AU), Wright-Patterson AFB OH, December 1990.

12. I.S.Gradshteyn and I M Ryzhik. *Table of Integrals, Series, and Products* (Fourth Edition) San Diego, CA: Academic Press, Inc., 1980.

13 Kaylor, R "The Brave New World of Stealth Warfare," *U.S. News & World Report, 20-28* 22-23 (28 Nov 1988)

14 Kent, William J. *Plane Wave Scattering by Thin Linear Dielectric-coated Wires and Dielectric Strips A Moment Method Approach with Physical Basis Functions*. PhD dissertation, The Ohio State University, Columbus OH, 1985 (ON8518971).

15. Kent, William J. "2-D Coated Strip (Revisited)." Unpublished Notes, October 1989.

16 Müller, David E "A Method for Solving Algebraic Equations Using an Automatic Computer," *Mathematical Tables and Other Aids to Computation, 10*.208-215 (1956)

17. Olver, F.W.J. "Bessel Functions of Integer Order." In Abramowitz, Milton and Irene Stegun, editors, *Handbook of Mathematical Functions*, Washington, D C. U S. Government Printing Office, 1972

18 Richmond, Jack H. *Surface Waves on Plane Dielectric Sheets and Sandwiches* Contract AF 33(616)-5410, Columbus OH: The Ohio State University Research Foundation, September 1958.

19. Richmond, Jack H. *Scattering by Thin Dielectric Strips.* Contract NSG1613, Columbus OH The Ohio State University ElectroScience Laboratory, August 1983.

20 Richmond, Jack H. "Scattering by Thin Dielectric Strips," *IEEE Transactions on Antennas and Propagation, AP-33* 64-68 (January 1985).

21. Rogers, Capt Steven W. *Radar Cross Section Prediction for Coated Perfect Conductors with Arbitrary Geometries.* MS thesis, AFIT/GIM/LSM/86S-153, Massachusetts Institute of Technology, Cambridge MA, June 1986 (AD-A1709730).

22 Rojas, Roberto G. "Scattering by an Inhomogeneous Dielectric/Ferrite Cylinder of Arbitrary Cross-Section Shape - Oblique Incidence Case," *IEEE Transactions on Antennas and Propagation, AP-36*:238-246 (February 1988).

23. Sabalos, John N. and Gary A. Thiele. *On the Application of the GTD-MM Technique and Its Limitations.* Contract F1962878C0198. Columbus OH. The Ohio State University Electro-Science Laboratory, July 1980.

24 Sarkar, Tapan K. et al. "On the Choice of Expansion and Weighting Fuunctions in the Numerical Solution of Operator Equations," *IEEE Transactions on Antennas and Propagation, AP-33*:988-996 (September 1985).

25. Schelkunoff, S. A. "Anatomy of "Surface Waves"," *IRE Transactions on Antennas and Propagation*, pages S133-139 (December 1959).

26. Thiele, Gary A and Thomas H. Newhouse. "A Hybrid Technique for Combining Moment Methods with the Geometrical Theory of Diffraction," *IEEE Transactions on Antennas and Propagation, AP-23*:62-69 (January 1975).

27. Woodworth, Margaret B. *Large Matrix Solution Techniques Applied to an Electromagnetic Scattering Problem.* Contract F19628-86-C-0104, Waltham MA ARCON Corporation, November 1988.

28 Zheng, Wenxin and Staffan Strom. "The Null Field Approach to Electromagnetic Scattering from Composite Objects - The Case of Concavo-convex Constituents," *IEEE Transactions on Antennas and Propagation, AP-37*:373-383 (March 1989).

Vita

Captain William D. Wood, Jr., was born on 10 April 1963 in Fairfax, Virginia. He graduated from W. T. Woodson High School in 1981 and entered the University of Arizona, from which he graduated with honors in May 1985, receiving the degree of Bachelor of Science in Electrical Engineering and a commission through the Air Force Reserve Officer Training Corps. He was assigned to the Avionics Laboratory, Wright-Patterson AFB, Ohio, where he served as a fire control engineer developing air-to-air fire control algorithms, space-based kinetic energy weapon simulation software, and non-cooperative target recognition technologies. In May 1989 he entered the School of Engineering, Air Force Institute of Technology, specializing in Low Observables technology.

Permanent address: 262 North Delmar Avenue
Dayton, Ohio 45403

REPORT DOCUMENTATION PAGE

Form Approved
OMB No 0704 0188

1 AGENCY USE ONLY (Leave blank)	2 REPORT DATE	3 REPORT TYPE AND DATES COVERED
	December 1990	Master's Thesis

4 TITLE AND SUBTITLE

TE Scattering From A Dielectric-Coated Conducting Strip

5 FUNDING NUMBERS

6. AUTHOR(S)

William D. Wood, Jr., Capt, USAF

7 PERFORMING ORGANIZATION NAME(S) AND ADDRESS(ES)

Air Force Institute of Technology
Wright-Patterson AFB OH 45433-6583

8 PERFORMING ORGANIZATION REPORT NUMBER

AFIT/GE/ENG/90D-67

9 SPONSORING/MONITORING AGENCY NAME(S) AND ADDRESS(ES)

10 SPONSORING MONITORING AGENCY REPORT NUMBER

11. SUPPLEMENTARY NOTES

12a DISTRIBUTION/AVAILABILITY STATEMENT

12b DISTRIBUTION CODE

13 ABSTRACT (Maximum 200 words)

Consider a plane wave incident on a conducting strip of infinite length coated on one side with a thin, uniform coating of lossless dielectric, and let the incident magnetic field vector be parallel to the edges of the strip. From first principles we develop the integral equations relating the total, incident, and scattered fields in the dielectric. We expand the fields in the dielectric slab as the sum of three plane waves (the "forced" wave and two oppositely-directed surface waves). The phase constants in the x and y directions are known and the wave amplitudes are found using least-squared-error point-matching. The far-zone scattered field is found by letting the polarization and conduction currents radiate in free space.

Data are presented showing the bistatic scattering characteristics of the dielectric-coated conducting strip as a function of dielectric permittivity, slab width and thickness, and angle of incidence. Results show reasonable agreement with conventional moment method solution using pulse bases and Galerkin testing functions.

14 SUBJECT TERMS	15 NUMBER OF PAGES
Electromagnetic Scattering; Physical Basis Functions Method of Moments; Radar Cross Section; Dielectric	77
	16 PRICE CODE

17 SECURITY CLASSIFICATION OF REPORT	18 SECURITY CLASSIFICATION OF THIS PAGE	19 SECURITY CLASSIFICATION OF ABSTRACT	20 LIMITATION OF ABSTRACT
Unclassified	Unclassified	Unclassified	UL